Afonso Mendes Ferreira

Licenciado em Engenharia Eletrotécnica e Computadores

Massive MIMO transmission techniques

Dissertação para Obtenção do Grau de Mestre em

Engenharia Eletrotécnica e Computadores

Orientador:	Prof. Doutor Paulo Montezuma, Professor Auxiliar, FCT-UNL
Co-orientadores:	Prof. Doutor Rui Dinis, Professor Associado com Agregação, FCT-UNL

Júri:

Presidente:	Prof. Doutor Nuno Paulino, Professor Auxiliar, FCT-UNL
Arguente:	Prof. Doutor Luís Bernardo, Professor Auxiliar com Agregação, FCT-UNL
Vogal:	Prof. Doutor Paulo Montezuma, Professor Auxiliar, FCT-UNL

Setembro de 2016

FACULDADE DE CIÊNCIAS E TECNOLOGIA
UNIVERSIDADE NOVA DE LISBOA

Massive MIMO transmission techniques

Aos meus pais e aos meus avós, que sempre lutaram por mim…

Acknowledgments

First of all, I wish to express my sincere thanks to Professor Paulo Montezuma for his constant encouragement, scientific knowledge and invaluable work over the past months, which made this dissertation possible. I would also like to thank Professor Rui Dinis for helping in problem solving and clarification of doubts. My appreciation to Faculdade de Ciências e Tecnologias da Universidade Nova de Lisboa, a great university where I learned so much more than my engineering course. Finally, my thanks to my parents who have always supported me and to my good friend Guilherme Gaspar, who was always present throughout this journey. I also place on record, my sense of gratitude to one and all who, directly or indirectly, have lent their helping hand in this venture.

Abstract

Next generation of mobile communication systems must support astounding data traffic increases, higher data rates and lower latency, among other requirements. These requirements should be met while assuring energy efficiency for mobile devices and base stations.

Several technologies are being proposed for 5G, but a consensus begins to emerge. Most likely, the future core 5G technologies will include massive MIMO (Multiple Input Multiple Output) and beamforming schemes operating in the millimeter wave spectrum. As soon as the millimeter wave propagation difficulties are overcome, the full potential of massive MIMO structures can be tapped.

The present work proposes a new transmission system with bi-dimensional antenna arrays working at millimeter wave frequencies, where the multiple antenna configurations can be used to obtain very high gain and directive transmission in point to point communications. A combination of beamforming with a constellation shaping scheme is proposed, that enables good user isolation and protection against eavesdropping, while simultaneously assuring power efficient amplification of multi-level constellations.

Keywords: mmWave, Massive MIMO, Beamforming.

Resumo

A próxima geração de sistemas de comunicações móveis terá de suportar um aumento enorme de tráfego de dados, maiores ritmos de transmissão e menor latência, entre muitos outros requisitos. Estes requisitos devem ser cumpridos enquanto os dispositivos móveis e estações base permanecem eficientes energeticamente.

Diversas tecnologias diferentes estão a ser propostas para o 5G mas um consenso perante as principais tecnologias a adotar começa a emergir. Muito provavelmente, sistemas *massive MIMO* (Multiple Input Multiple Output) com esquemas de diretividade a operar no espectro de ondas milimétricas formarão a base tecnológica do 5G. À medida que as dificuldades de propagação das ondas milimétricas são superadas, todo o potencial de estruturas *massive MIMO* pode ser aproveitado.

A presente dissertação propõe um novo sistema de transmissão com vectores bi-dimensionais de antenas que operam em frequências de ondas milimétricas, onde as múltiplas configurações de antenas podem ser utilizadas para obter ganhos muito elevados e transmissões directivas em comunicações ponto a ponto. Além destas vantagens, é proposta uma combinação de directividade na transmissão e na informação, permitindo maior isolamento entre utilizadores e proteção contra interceção e espionagem, assegurando também simultaneamente a amplificação eficiente de constelações multinível.

Palavras-chave: *mmWave*, *Massive MIMO*, Directividade.

Contents

Table Index

Figure Index

1 Chapter I– Introduction

In the past few years, discussions about possible 5G standards have been the focus of telecommunications researchers and engineers around the world. As Long Term Evolution (LTE - 4G) systems are reaching full capacity, the research and definition of new technologies seems a critical issue.

Next generation of wireless communications systems will have to deal with new challenges and requirements driven by multiple perspectives of society, environment and economy to achieve success [1]. Academies and industries are engaging in multi-national collaborative projects, such as Mobile and wireless communications Enablers for Twenty-twenty Information Society II (METIS II) to develop new technologies in order to meet the intense demand of more traffic. These key technologies for 5G networks go beyond physical layer transmission and channel encoding, but also ponder more innovations such as multi-points, multi-users, massive Multiple Input Multiple Output (MIMO), multi-cell cooperation and higher-level spectral efficiency [1].

This dissertation proposes a new multilayer transmission system with bi-dimensional antenna arrays working at millimeter wave frequencies, using multilevel modulations. Due to the short wavelengths of millimeter waves, large numbers of antennas can be deployed in small areas, which allows the use of multiple antenna systems to obtain very high transmission gains, with beamforming and massive MIMO techniques [2].

Beamforming is a versatile technique for signal transmission in the presence of noise or interference, assuring high data rates [3]. Unfortunately, in practice, the limited number of transmission antennas cannot guarantee perfect directivity, which means that users are still somewhat interfering. Although designing a beamforming vector that maximizes the signal power at the intended user is fairly easy, minimizing interference at the same time is generally a nondeterministic polynomial-time (NP) hard problem [4].

The use of multilevel modulations provides increased spectral efficiency, but comes at the expense of reduced power efficiency, which is undesirable as all 5G systems must be energetically efficient [5].

So, power and spectral efficiencies are contradictory requirements, as high spectral efficiency means using large constellations with high envelope fluctuations. Amplification efficiency, on the other hand, requires the use of nonlinear amplifiers, which only work with constant or almost constant envelope signals when it is intended to avoid nonlinear distortion.

Also, it is well known that large or non-uniform constellations are sensitive to interference, specifically ISI (Intersymbol Interference) caused by multipath propagation and dispersive channel effects. To invert channel effects, the use of a SC-FDE (Single-Carrier with Frequency-Domain Equalization) scheme was considered, which also has less envelope fluctuations and PAPR (Peak-to-Average Power Ratio) than OFDM (Orthogonal Frequency-Division Multiplexing), contributing to efficient amplification.

The proposed multi antenna transmitter combines beamforming with a constellation shaping technique. Optimizing the constellation to the desired direction enables greater user isolation and protection against eavesdropping. This is achieved by decomposing multilevel constellations such as M-Quadrature Amplitude Modulation (M-QAM) constellations as the sum of Quadrature Phase Shift Keying (QPSK) or polar components. These components with constant or almost constant envelope are amplified and transmitted independently by one antenna array directly connected to the amplifier of each branch [5]. Therefore this transmitter structure combines the use of nonlinear amplifiers, which have lower complexity and higher efficiency, with the spectral efficiency of larger QAM modulations [6].

The strategy is to blend both techniques in a bi-dimensional antenna array composed by $N_v \times N_h$ antennas, where N_v and N_h denote the antenna elements aligned vertically and horizontally, respectively. The N_v elements are responsible for the constellation shaping (layer 1) and the N_h elements are responsible for azimuthal radiation directivity (layer 2). For proper reception, the receiver not only needs to be in the direction of maximum radiated power, but also needs to know the constellation parameters and array configuration, otherwise it receives a degenerate signal. Consequently, robustness against interception and interference is enhanced.

The technology described above is particularly suitable for 5G wireless communications as it can take advantage of the large number of antennas the millimeter wave spectrum enables, providing azimuthal power directivity and reinforced security against interception. This is jointly combined with massive MIMO techniques and support for an increased number of users, while simultaneously assuring power efficiency for large multilevel constellations.

After this introductory part, the rest of the thesis is organized as follows:

Chapter II presents a brief explanation of what's expected of 5G and the possible technologies behind it, namely, millimeter wave spectrum, massive MIMO and beamforming. Also, a brief description of channel time and frequency selectivity is made.

Chapter III addresses the beamforming and multi-array transmission structures, as well as the limitations regarding bi-dimensional optimizations of the radiation patterns. A set of results regarding the optimization of such emission structures is also presented.

Chapter IV characterizes the multilayer transmitter architecture that combines spatial radiation pattern optimization with constellation shaping based on the decomposition of multilevel constellation into a sum of polar components that are separately amplified. Multi-carrier block transmission and Single Carrier with Frequency Domain Equalization (SC-FDE) are analyzed, and a SC-FDE scheme is applied together with several configurations of the multilayer approach. For each one a set of simulation results is also presented.

Finally, chapter V concludes this thesis with some guiding lines for future work.

2 Chapter II – State of the art

This chapter contextualizes this thesis under 5G. Firstly, a brief overview of the major milestones and progress in wireless telecommunications up to 5G is made in section 2.1. The expected prerequisites for all future 5G networks are explained in section 2.2 along with the major emergent technologies to achieve such ambitious goals, namely, millimeter wave spectrum, massive MIMO and beamforming. Lastly, section 2.3 consists in a brief study of channel selectivity, introducing as well the subject of block transmission techniques, particularly OFDM and SC-FDE.

2.1 Leading to 5G

Every decade or so, a new generation of mobile network technology is released. The first generation, Nordic Mobile Telephone, appeared in the 1982, 2G followed in 1992, 3G arrived at 2001 and 4G systems fully compliant with The International Mobile Telecommunications (IMT Advanced) began to be implemented in 2012. The 5G denotes the next major phase of mobile telecommunications standards beyond the current 4G.

First generation cellular networks were analog systems, aimed for voice communications. Data services and improved spectral efficiency were introduced in 2G systems by using digital modulations and time/code division multiple access technologies. 3G introduced high speed mobile Internet access, video calls and mobile TV services. Later 3G releases, often denoted 3.5G and 3.75G can provide data rates of several Mbps using Wideband Code Division Multiple Access (W-CDMA) and the latest Evolved High-Speed Packet Access (HSPA+) technologies.

In parallel with HSPA, LTE radio access technology has been developed by the 3rd Generation Partnership Project (3GPP) to offer a 4G mobile broadband platform [7]. LTE uses Orthogonal Frequency Division Multiple Access (OFDMA) and Single Carrier Frequency Division Multiple Access (SC-FDMA) technology that supports multi antenna transmission and spectrum flexibility. LTE had a number of upgrades since its release, and LTE Release 10, known has LTE-Advanced, extends LTE capabilities in a number of ways and allows peak data rates of 3 Gbps [7].

A growing consensus among the researchers is that 4G still has considerable lifetime, considering LTE and LTE-Advanced are just being deployed. In fact, these technologies should continue to evolve in terms of higher speeds and greater capacity.

When will 5G be implemented? What are the technologies and solutions that will be used? These are the most discussed topics among mobile operators, research institutions, trade organizations and governments. According to [8] and [9] we can expect 5G standards to be introduced in the early 2020s.

Until now, each generation aims to fix the shortcomings of its antecedent and is characterized by new frequency bands, higher data rates and a new technological shift that breaks backward compatibility. However, for the fifth generation, some sources suggest that although technological modifications are required, compatibility is essential, tying the new 5G air interface with LTE and WiFi to provide higher rates and better coverage [10]. To achieve this, changes at the core network, spectrum regulation and energy efficiency must be considered [11].

In order to fully comprehend the engineering challenges ahead, it is essential to identify the expected requirements of the technology. As mentioned before, the industry is defining these requirements for deployment in the 2020s without an actual technology developed. With that in mind, some requirements may not be achievable in the expected timeframe.

2.1.1 What to expect from 5G?

Traffic volume growth

The main drive for 5G development and evolution is the foreseeable astounding data traffic increase for the near future.

The annual visual network index report (VNI) made by Cisco shows that the wireless data explosion is here to continue. Just in 2014 alone, global mobile traffic grew 69% and reached 2.5 Exabyte per month compared to the 1.5 Exabyte from 2013, and almost half a billion (497 million) mobile devices and connections were added. This growth rate will rise and overall mobile data traffic is expected to grow to 24.3 Exabyte per month by 2019, nearly a tenfold increase over 2014, as shown in figure 2.1 [12].

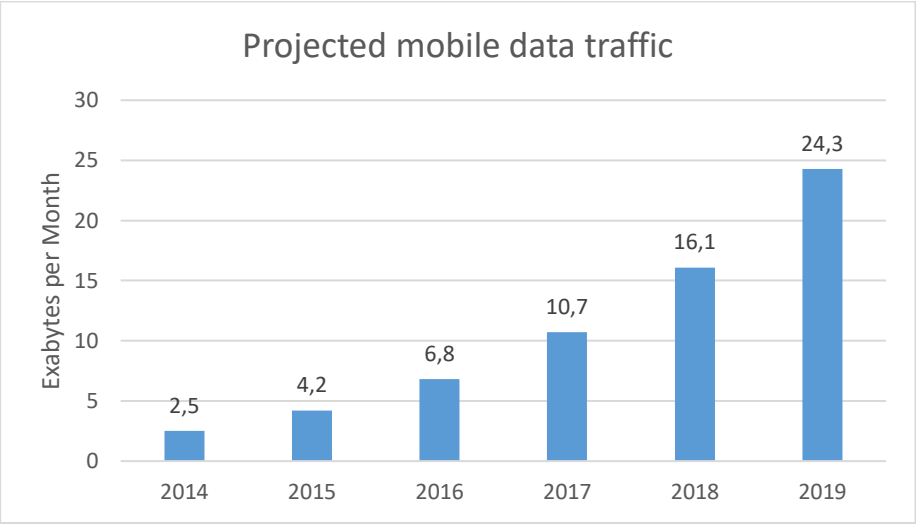

Figure 2.1 – Global mobile data traffic per month forecast

3G and 4G technologies are focused mainly on providing enhanced system capacity and higher data rates, but 5G brings more than the conventional mobile broadband use. Future wireless networks should offer wireless access beyond humans and allow objects to collect and exchange data for a wide range of new applications and use cases, including wearables, smart homes, traffic control and critical services. This is usually called the Internet of Things (IoT) or machine-to-machine communication (M2M). A Massachusetts Institute of Technology (MIT) study from 2014, represented in figure 2.2, projected that by 2020 there will be 26 billion objects connected to the Internet [13].

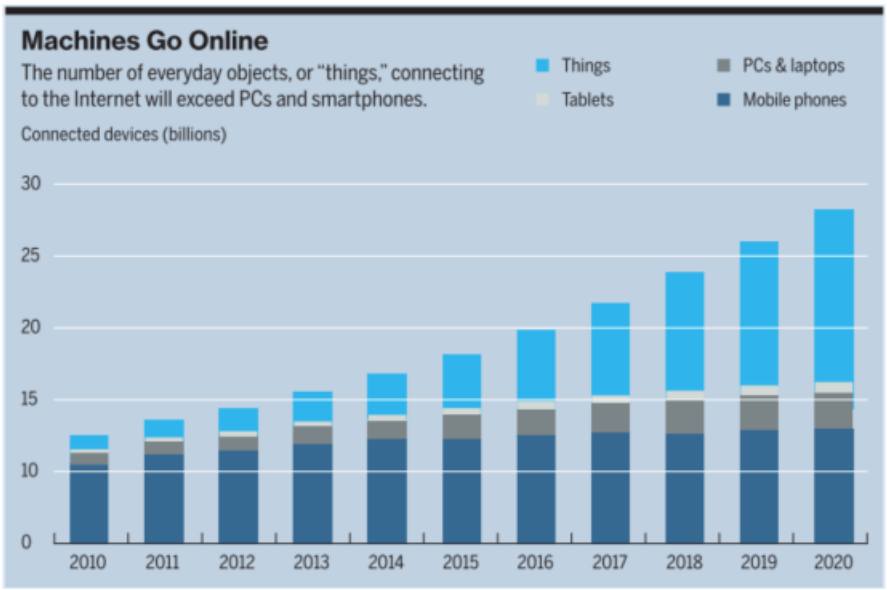

Figure 2.2 - Forecast of miscellaneous objects connecting to the Internet, from [13]

5G network elements need to scale up to handle this growth, especially when supporting a mix of traffic from IoT applications and more traditional voice and video services. For example, a single macro cell may need to support thousands of low-rate M2M devices along with the traditional high-rate mobile users. Current radio networks, based on a mixture of Global System for Mobile Communications (GSM), Universal Mobile Telecommunication System (UMTS) and LTE, as well as WiFi for hotspot scenarios, cannot keep pace with the demand [14].

Higher data rate

5G should be able to provide data rates superior to 10 Gbps in indoor scenarios and dense outdoor environments, data rates of several 100 Mbps should be achievable in urban or suburban environments and at least 10 Mbps should be possible virtually anywhere, including rural and remote areas [10].

These requirements represent an advance about one hundred to a thousand times above current 4G capabilities[15].

Energy efficiency

Despite the expected increase in data traffic, the network must stay competitive and energy consumption should decrease, or at least maintain on a per-link basis. In addition to maximizing spectral efficiency, the energy per bit should be minimized. Also, network functions must not convey excessive energy, either radiated or consumed by network infrastructure. This is an important issue to reduce operational costs, allowing a sustainable and resource efficient network.

Significant energy savings in off-peak situations can be obtained through a regulation of energy consumption according to current traffic conditions.

Latency

For some of the envisioned 5G applications, such as traffic control, critical infrastructure monitoring, public safety, virtual reality and gaming, reducing latency is vital. The unanimous opinion among researchers is that 5G standards should have less than 1 millisecond of latency for both downlink and uplink [10], [15], [14], about an order of magnitude faster than 4G.

Seamless Mobility

5G core network shall support seamless mobility among all cell types, such as environments where macro, small and personal cell base stations are mixed and/or overlapped with WLAN networks.

Current mobile core networks are mainly designed to support macro cell handover and since the future mobile core networks ought to support various wireless accesses in the common platform, the seamless handover between the different types of access is a paramount requirement. Also, the ability to provide handover between wireless and wired terminals should be assured.

Single ID for multiple access

The 5G core network shall always provide the best connection/service. In current cellular systems, the network makes the cell selection based on the radio signal quality that shares the same access technology. When multiple access technologies (i.e. 5G macro cell Base Station (BS) and Wireless Local Area Network (WLAN)) are available, the network shall recognize a mobile terminal as a single entity (same ID for all wireless interfaces) regardless of access type and support service continuity and mobility.

2.2 Potential technologies for 5G

2.2.1 Millimeter wave (mmWave)

Current mobile communications networks operate with carrier frequencies between 700 MHz and 2.6 GHz, corresponding to centimeter wavelengths. Nowadays, these frequency bands are completely occupied, and in order to achieve the proposed capacity and data rates, enhancing spectral efficiency it's not enough, more Hz are needed [16]. The only place to go for more bandwidth are higher frequencies, where vast amounts of free spectrum is available in the millimeter wavelength range of 30 to 300 GHz.

These frequency bands have several hundred continuous unoccupied MHz, which allow larger bandwidth allocations, needed to support multiple Gbps data rates. Although still unclear what frequency bands will be allocated for 5G, a range from 10 GHz to 100 GHz is being considered [10], along with some bands below 6 GHz, represented in figure 2.3.

Figure 2.3 - Spectrum range for 5G

The main drawbacks of using higher frequencies are higher free space propagation losses, reduced diffraction around objects and poor penetration through obstacles.

Thus, the focus of previous study in this area restrained to short range wireless communications such as point to point systems and LANs [18]. In December 2012, the first standard for millimeter wave communications was issued (IEEE 802.11ad), providing up to 6.75 Gbps throughput using approximately 2 GHz of spectrum at 60 GHz over a LAN within a room [17].

However, free space loss is not linear, as for higher frequencies the attenuation becomes more dependent on certain absorbing characteristics of atmospheric components, mainly oxygen and water. As shown in figure 2.4, attenuation at marked spectrum regions is approximately only one order of magnitude higher than the lower frequencies, which makes those regions suitable for cellular communications.

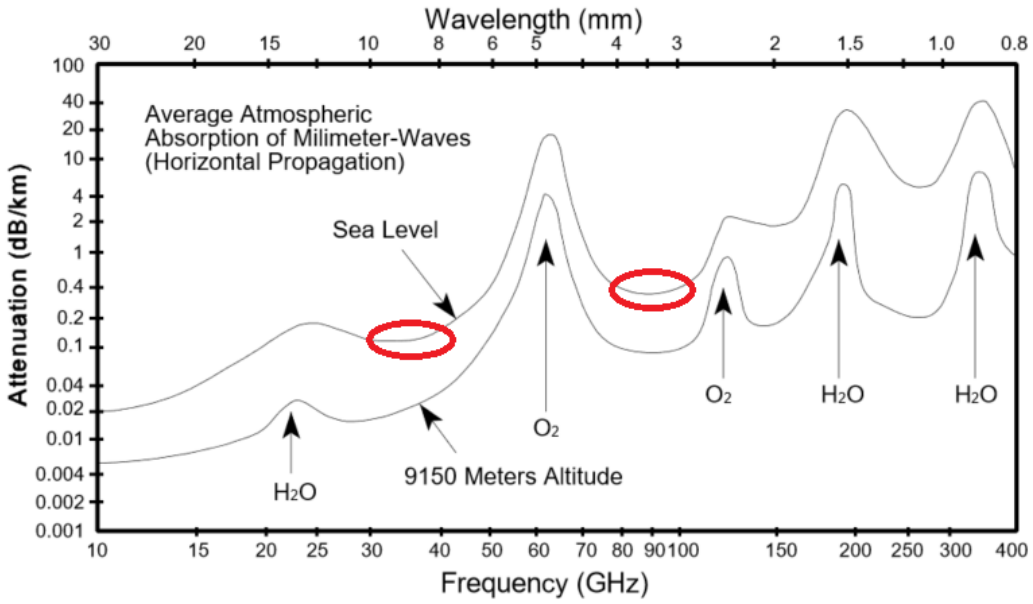

Figure 2.4 - Milimeter wave atmospheric absorption, marked red zones are possible frequencies allocated for 5G, from [19]

Test results by Nippon Telegraph and Telephone Corporation (NTT Docomo) show that the path loss exponent, delay spreads and angle spreads of millimeter wavelengths bands are comparable to those of typical cellular frequency bands, when transmit and receive antennas are used to produce beamforming gains. As millimeter wavelengths enable large numbers of antennas to be deployed in small areas and as Complementary Metal–Oxide–Semiconductor (CMOS) technology develops and gets cheaper, more and more antennas can be applied at base stations or within cell phones [20].

Nevertheless, the viability of mmWave transmissions still faces serious technical problems. Although omnidirectional path loss can be compensated by beamforming and directivity, mmWave signals are susceptible to shadow fading, which can cause outages and intermittent channel quality. [20]. Also, difficulties with the manufacture of small elements and device power consumption are to be considered [21].

As operators continue to reduce cell coverage areas to gain advantage of spatial frequency reuse, the cost per base station drops as they increase in number and become more densely distributed. Thus, the focus of 5G millimeter wave deployments will be in small (few hundred meters) size urban cells or hot spot environments [22]. These cell densities are becoming common place under 4G deployments and mmWave will upgrade throughput at these small cell scenarios [21].

While extra widespread measurement campaigns are being supported out all over the world to build a comprehensive statistical mmWave channel propagation model [23], it is apparent that the mmWave bands are a strong candidate for the next generation cellular networks. After further study of the channel model, the next step is to develop the core technologies to efficiently take advantage of the abundant mmWave spectrum and prove their commercial viability.

2.2.2 Massive MIMO

MIMO is a method that increases the capacity of a radio link by using multiple transmit and receive antennas to exploit multipath propagation. This technology outperforms conventional Single-Input, Single-Output (SISO) systems and is now incorporated in current wireless systems, including Wi-Fi, HSPA+, WiMAX, LTE and some power line communication applications [24]. MIMO consists in sending and receiving more than one data signal on the same radio channel, at the same time. Spatial multiplexing techniques can increase data rates and channel fading can be mitigated by employing receive and transmit diversity [25].

The more antennas the transmitter/receiver has, the better performance in terms of data rate or link reliability [26]. However, MIMO systems have increased hardware complexity and need considerable physical space area, as one of the main factors impacting MIMO performance is the distance between antenna elements. This spacing impacts the mutual correlation of channel fading on signals from different antennas.

However, this relation between antenna spacing and fading mutual correlation is not the same at indoor or hotspot scenarios and at long range macro cell scenarios. At indoor and hotspot scenarios, the environment seen from the base station is similar to the environment seen from the terminal [27]. In this case, smaller spacing between antennas is needed to assure low mutual correlation among antennas, typically 0.5λ is used, with λ representing signal wavelength [27], which also is the optimum spacing to achieve directivity gains (beamforming).

With the ability to provide both MIMO and beamforming techniques to multiple users in one small cell, system capacity increases greatly, as illustrated in figure 2.5.

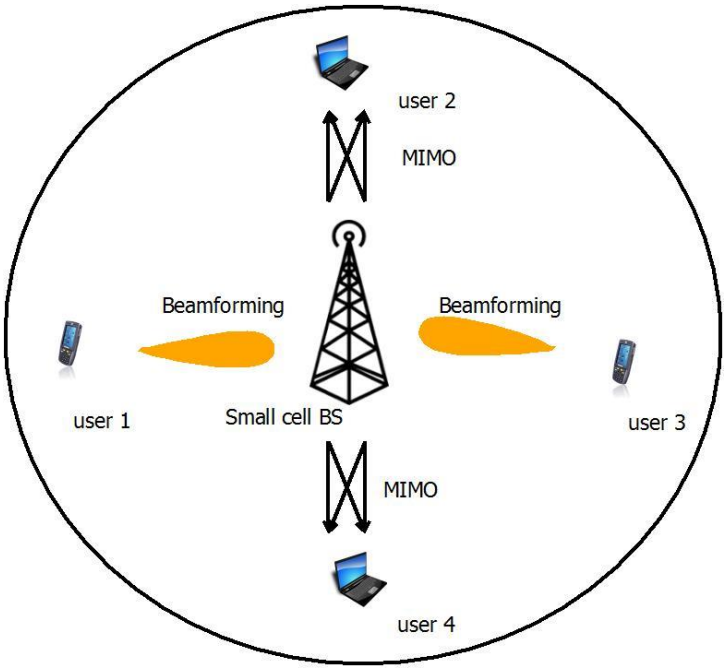

Figure 2.5 - Multiuser MIMO and beamforming examples at small cell level

In single user MIMO (SU-MIMO), the number of antennas is limited to the dimension of the mobile device (usually two to four antennas are used in current phones). Nonetheless, having the Base Station communicate with several users simultaneously enables the multiuser version of MIMO (MU-MIMO), often considered in literature as Space-Division Multiple Access (SDMA). SDMA

supports multiple users on a single channel, each one identified by different spatial signatures. Also, coordinated multipoint transmission/reception between multiple Base Stations can be seen as a single MIMO transceiver [28]. A basic configuration of MU-MIMO base station cooperation is depicted in figure 2.6. The main goal of this cooperation is the reduction of inter-cell interference.

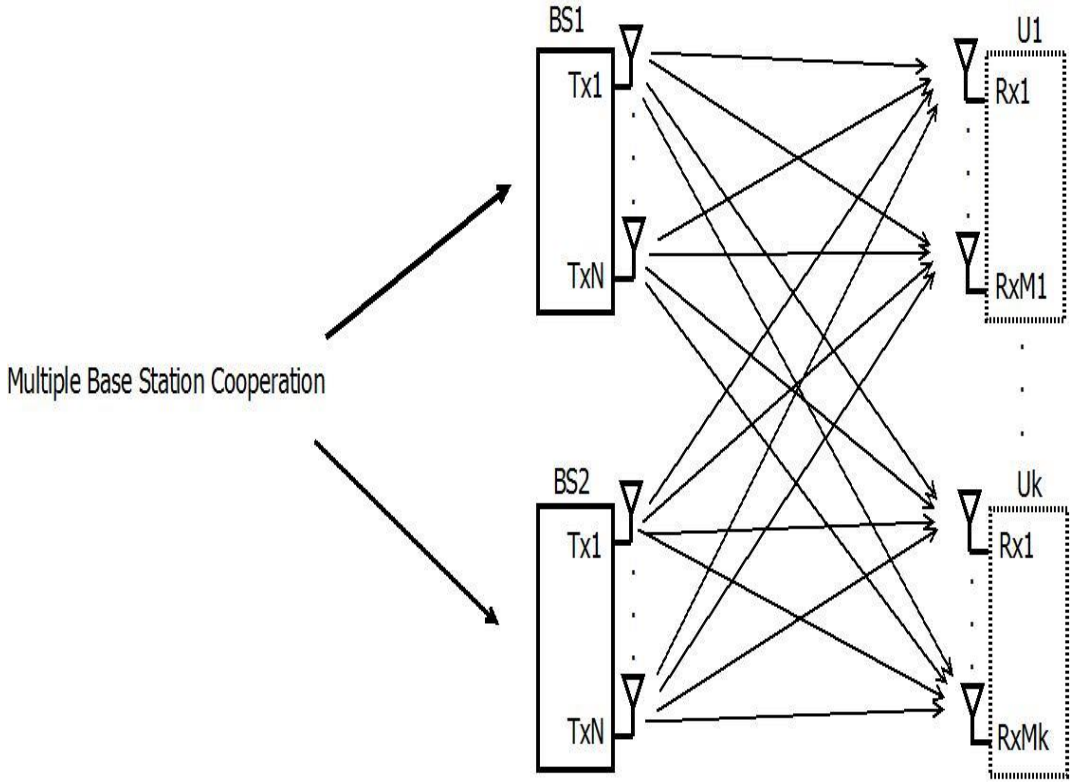

Figure 2.6–Downlink MU-MIMO communication with Base Station cooperation

In figure 2.6, the presented MU-MIMO system consists of two base stations BS1 and BS2 each equipped with N antennas. K users $U_1, \dots, U_K$ with $M_1, \dots, M_K$ antennas communicate with the cooperating BS1 and BS2. The fact that multiple users can communicate over the same frequency greatly increases system capacity, but are also subjected to strong Co-Channel Interference (CCI). Several approaches to cancel CCI have been proposed and will be addressed in depth in Section 4.3. MU-MIMO schemes find application in many current technologies, such LTE [29] and other cooperative multicellular networks [30].

In 2010, Marzetta proposed the extension of MIMO to a number of antennas at Base Stations much larger than the number of active users being served simultaneously in the same time-frequency block [31]. This approach to MU-MIMO is now known as massive MIMO and offers great benefits.

Using large number of antennas will guarantee high throughput, as precise beamforming will serve multiple users in the same cell. Furthermore, channel responses can be stabilized by virtue of vast spatial diversity and under reasonable propagation conditions, increasing the number of antennas permits the reduction of base station power [32].

Massive MIMO uses Time-Division Duplexing (TDD) and reciprocity in the uplink and downlink channels is advantageous, offering fast and accurate channel information. However, this reciprocity is only maintained in low mobility scenarios, typical of small cell applications (e.g. hotspots). The main challenge to massive MIMO is at macro cell scenarios, where high user mobility must be supported and it's difficult to quickly get accurate channel information. Therefore, in these cases performance improvements are limited [27].

2.2.3 Beamforming

As mentioned before, higher frequencies present propagation challenges but also offer opportunities. As the carrier frequency becomes higher, the antenna elements can be smaller and more elements can be packed into antenna aggregates. These large numbers of antenna elements can create highly directional beams, corresponding to large array gains.

As millimeter wave systems can take advantage of the combination of small cell networks and massive MIMO schemes, beamforming at transmission and reception can be used to handle characteristic propagation losses and support large numbers of co-channel users. Beamforming is realized by combining antenna elements in a phased array in such a way that signals power is reinforced or reduced at particular transmission angles. To change the directionality of the antenna array, the phase and relative amplitude of the signal at each element are controlled, in order to create a pattern of constructive and destructive interference in the wave front.

Depending on the beamforming architecture, the beamforming weights required to form the directive beam can be applied in the analog or digital domain. Digital beamforming consists in digital precoding that multiplies a specific coefficient to the modulated baseband signal per radio frequency (RF) branch. Analog beamforming, on the other hand, complex "weight" coefficients are applied, controlling phase shifters and/or variable gain amplifiers (VGAs).

Non-uniform weighting algorithms, such as Chebyshev and Taylor, can be used to control main lobe width and side lobe levels or force the position of nulls, which can provide isolation from noise or signal jammers from those directions.

Overall, digital beamforming offers better performance at the expense of higher complexity and cost, due to the fact that separate digital-to-analog converters (DACs) and analog-to-digital converters (ADCs) are required for each RF branch. On the other hand, analog beamforming is simpler and effective for generating high gains but less flexible, and while a promising addition to downlink transmission in this 5G antenna massification context, traditional analog beamforming is still subjected to a number of constraints and disadvantages. Namely, the incompatibility with spatial multiplexing and high dependence on very large number of antennas for worthwhile gains and user isolation, enabling frequency re-use and increased system capacity. Chapter III studies in more depth unidimensional and bi-dimensional antenna array beamforming and the corresponding performance limitations.

The trade-off between performance and simplicity pushes the need for hybrid architectures, especially in millimeter wave bands [33].

Figure 2.7 illustrates a possible hybrid beamforming architecture applied at the transmitter for the downlink. In this architecture, analog beamforming directs transmission and compensates path loss, and digital beamforming enables multi user MIMO by cancelling co-channel interference.

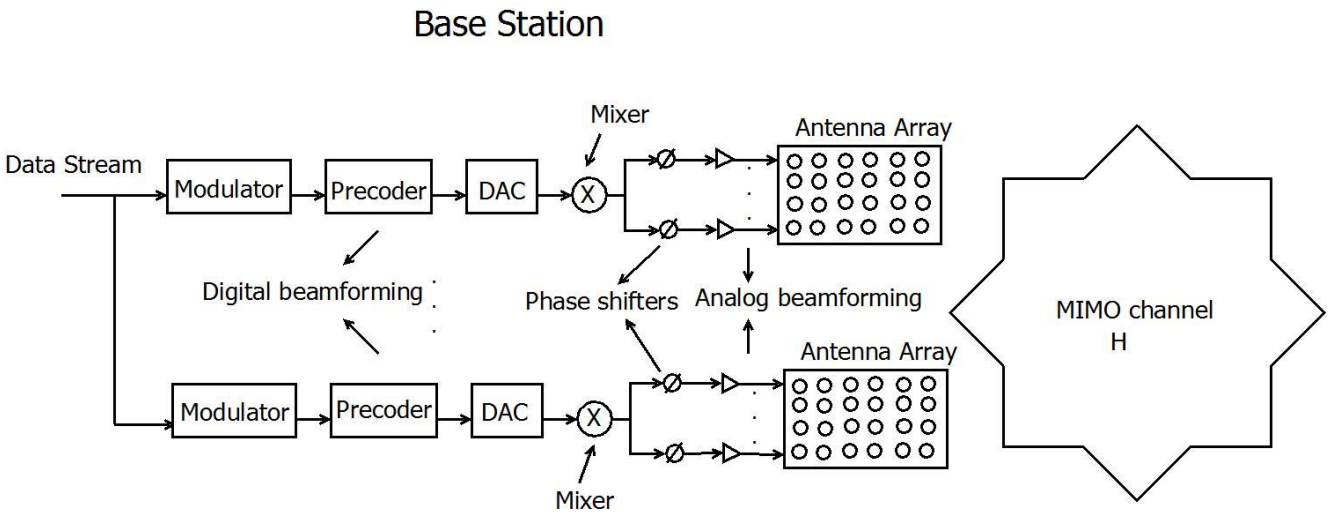

(a)

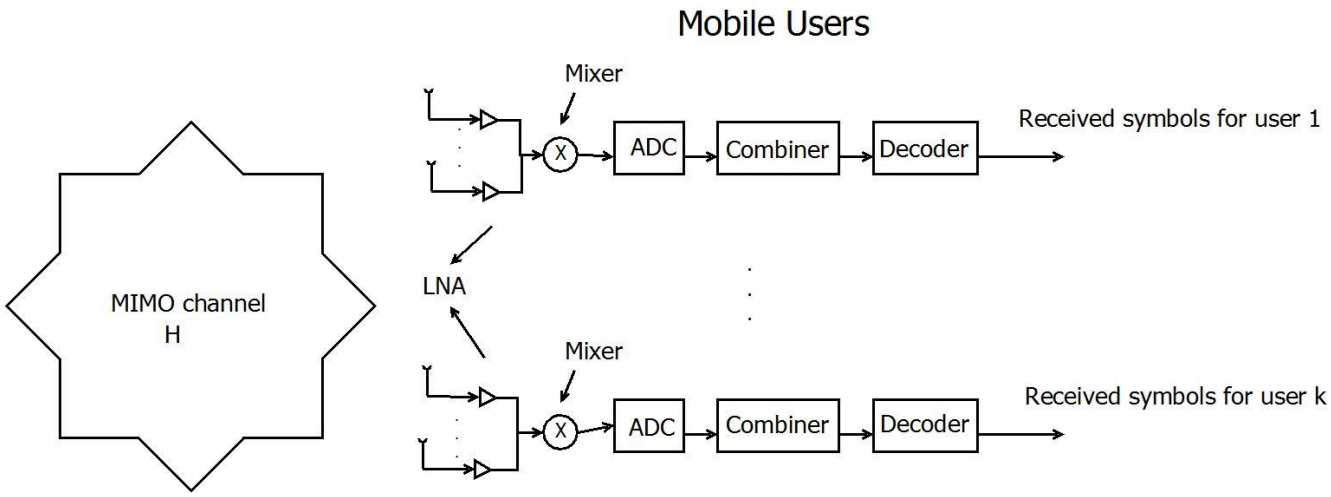

(b)

Figure 2.7–Hybrid beamforming architecture for the downlink scenario with receive diversity for multiple users. (a) represents the transmitter and (b) represents the receivers

Using a similar hybrid beamforming scheme, a recent Samsung's prototype [15], operating at 28 GHz, uses a 64 phased antenna array both on transmitter and receiver, generating a beam 10 degrees wide that can be steered in any direction. Base station then scans for the strongest connection, getting around objects by taking advantage of reflections. This prototype was able to provide data rates of 1056 Mbps to a receiver moving at 8km/h without line of sight. At maximum transmission range of 2 km with line of sight at indoor to outdoor scenarios, and vice versa, penetration tests exhibited promising results, with block error ratios (BLERs) inferior to 0,6%. A similar study made by New York University [22], also working at 28 GHz, achieved similar results in NYC dense urban environment.

These initial test results prove that millimeter wave hybrid beamforming can be a strong candidate to deal with the massive 5G requirements, and provide solid ground for further development. However, nothing comes without cost and enabling these systems in practice requires dealing with channel impairments and system design difficulties. The main propagation-related difficulties in millimeter wave cellular networks are that free-space path loss is larger at higher frequencies and non-line-of-sight paths are weaker, making blockage and coverage holes more prominent. To overcome blockages, in addition to using steerable arrays, networks can be made very dense with a heterogeneous infrastructure that can include smaller cells.

The system design problems come associated with high carrier frequency and wide bandwidth that can cause severe nonlinear distortion of power amplifiers, phase noise and In-phase and Quadrature (IQ) imbalance [34]. Also, due to transmission directivity, coordination mechanisms become key to the Medium Access Control (MAC) layer design and concurrent transmission should be exploited to increase network capacity [35].

The proposed multilayer transmitter architecture in Chapter IV combines a similar hybrid beamforming structure with added information directivity, enabling greater physical layer security against eavesdropping while guaranteeing amplification efficiency for large multilevel constellations.

2.3 Time and frequency selective channels

In wireless communication systems, the transmitted signal can propagate through several different paths to the receiver. This is usually caused by the reflection of radio waves from surrounding buildings or other obstacles and is usually called multipath propagation. Each multipath component has different propagation delays and attenuations, which means that the overall received signal frequencies of the modulated waveform can experience different attenuations and phase variations. This phenomenon is known as frequency selective fading. If the transmitter or the receiver are mobile, or some other kind of time varying behavior affects the propagation environment, the radio channel is also time variant, meaning that variable time delays may affect each multipath component. This is commonly known as time selective fading.

In order to better understand time and frequency selective fading, the concepts of coherence bandwidth and coherence time must be introduced. Coherence bandwidth is a statistical measurement over the range of frequencies in which the channel is flat. In other terms, coherence bandwidth is the maximum frequency interval in which multiple frequencies of a signal are affected by similar fading. If a channel delay spread is given by D seconds, representing the time difference between the arrival of the earliest and the latest multipath component, the coherence bandwidth Bc can be approximately given by$Bc \cong \frac{1}{D}$. It is intuitive to conclude that the channel is considered non frequency selective (flat) if the coherence bandwidth is greater than the signal bandwidth. Delay spread and, consequently, coherence bandwidth greatly affect the presence of ISI (Intersymbol Interference) as the symbol duration needs to be longer than the delay spread to ensure a ISI free channel.

Although delay spread and coherence bandwidth can describe frequency selective channels, these parameters do not offer any information about the time varying nature of the channel caused by relative motion between transmitter and receiver. For this effect, when a user is moving, the user's velocity causes a shift in the transmitted signal frequency along each multipath, known as Doppler shift. Different multipaths can have different Doppler shifts, corresponding to different rates of phase variations. The contributions of all Doppler shifts from all multipath components is known as the Doppler spread (Ds). As coherence time (Tc) is given by $Tc \cong \frac{1}{Ds}$, channels with high Doppler spread have large multipath phase variations and very short coherence time, which is the time duration over which the channel impulse response is not variable.

To conclude, if the signal bandwidth is greater than the coherence bandwidth of the channel, the channel is frequency selective. This means that some parts of the signal spectrum suffer different attenuation. At waveform level, the channel delay spread is larger than the symbol duration, which means strong ISI. Considering the time selectivity of the channel, the channel has slow fading if the channel's coherence time is larger than the signaling interval. This means an invariant channel over the symbol duration. However, if the coherence time is shorter than the signaling interval, the channel suffers fast fading, meaning accentuated channel changes during one signaling interval.

This frequency and time selective nature of mobile wireless channels is one of the most important aspects to assess wireless link quality and multiple transmitter and receiver processing techniques are used to overcome frequency and time selective fading in current wireless systems.

It is well known that Orthogonal Frequency Division Multiplexing (OFDM) is a good multicarrier solution for high data rate transmission over frequency selective channels. However, Cyclic-Prefix SC (CP-SC) based systems with FDE have similar performance, efficiency and low signal processing complexity advantages of OFDM, but in addition are less sensitive than ODFM to power amplifier nonlinear distortion effects [36]. Also, for double selective channels, an iterative equalization and compensation method has been proposed for SC wireless transmissions [37].

To cope with the frequency selectivity of broadband channels, it is considered an iterative SC-FDE scheme in this thesis, further explained in Chapter IV.

3 Chapter III – Antenna array analysis

3.1 Introduction

This chapter studies the properties of radiation directivity of unidimensional and bi-dimensional antenna arrays. First, a brief explanation of radiation patterns of a generic antenna array, along an azimuthal and elevation direction is extrapolated to a unidimensional array model of 16 antennas in section 3.2. This model is subsequently replicated 4 and 6 times in parallel, forming 4x16 and 6x16 bi-dimensional antenna arrays examined in detail in section 3.3.

To better comprehend radiation directivity, consider a linear antenna element. A linear antenna element (e.g. dipole) along the x-axis has omnidirectional pattern along the azimuthal angle ϕ and the elevation angle Θ. If the antenna is replicated along the x-axis, the omnidirectional pattern along the elevation angle Θ is preserved. With enough antennas, the main beam along ϕ can be narrowed and any desired gain pattern $g(\phi)$ can be achieved. Azimuth and elevation angles are represented in figure 3.1.

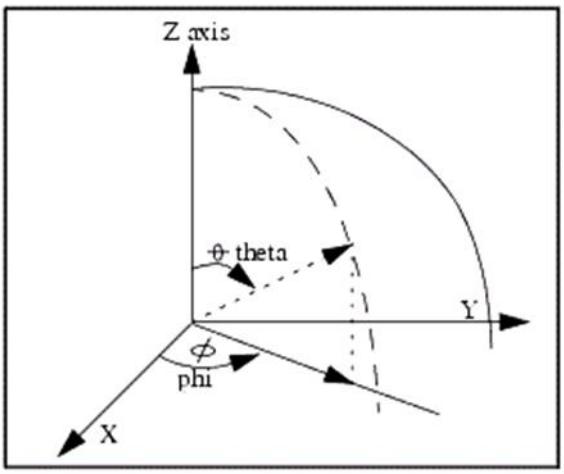

Figure 3.1 - Azimuth and elevation angle

Considering a multidimensional antenna array of n identical antennas located at positions $\boldsymbol{d}_0, \boldsymbol{d}_1, \boldsymbol{d}_2, \dots, \boldsymbol{d}_n$, and feed coefficients $a_0, a_1, a_2, \dots, a_n$. The corresponding radiation vector of the nth antenna comes:

$$\boldsymbol{F}_n(\boldsymbol{k}) = a_n e^{j\boldsymbol{k}\boldsymbol{d}_n} \boldsymbol{F}(\boldsymbol{k}), \tag{3.1}$$

and the total radiation vector:

$$\begin{aligned} \boldsymbol{F}_{tot}(\boldsymbol{k}) &= \boldsymbol{F}_0 + \boldsymbol{F}_1 + \boldsymbol{F}_2 + \cdots + \boldsymbol{F}_n \\ &= a_0 e^{j\boldsymbol{k}\boldsymbol{d}_0} \boldsymbol{F}(\boldsymbol{k}) + a_1 e^{j\boldsymbol{k}\boldsymbol{d}_1} \boldsymbol{F}(\boldsymbol{k}) + a_2 e^{j\boldsymbol{k}\boldsymbol{d}_2} \boldsymbol{F}(\boldsymbol{k}) + \cdots \\ &\quad + a_n e^{j\boldsymbol{k}\boldsymbol{d}_n} \boldsymbol{F}(\boldsymbol{k}). \end{aligned} \tag{3.2}$$

The factor $\boldsymbol{F}(\boldsymbol{k})$ due to a single antenna is common to all terms, so we can get the array pattern given by

$$\boldsymbol{F}_{tot}(\boldsymbol{k}) = A(\boldsymbol{k}) \boldsymbol{F}(\boldsymbol{k}), \tag{3.3}$$

where $A(\boldsymbol{k})$ is the array factor:

$$A(\boldsymbol{k}) = a_0 e^{j\boldsymbol{k}\boldsymbol{d}_0} + a_1 e^{j\boldsymbol{k}\boldsymbol{d}_1} + a_2 e^{j\boldsymbol{k}\boldsymbol{d}_2} + \cdots + a_n e^{j\boldsymbol{k}\boldsymbol{d}_n}. \tag{3.4}$$

$A(\boldsymbol{k})$ may also be denoted A(Θ,ϕ) and as noted in (3.3), the effect of the array of identical antennas is to multiply the single antenna radiation vector by the array factor, which includes the phase shifts and weight coefficients of all elements. The corresponded power gain is obtained similarly:

$$G_{tot}(\Theta, \phi) = |A(\Theta, \phi)|^2 G(\Theta, \phi), \tag{3.5}$$

where $G(\Theta, \phi)$ is the power gain of a single antenna.

3.2 Unidimensional antenna array

To study beamforming properties, a unidimensional array of 16 dipoles with uniform spacing ($d = \frac{\lambda}{2}$, with λ denoting wavelength) and uniform weights (**a**=[1, 1, ... , 1]) between elements was considered. The array layout is shown in figure 3.2.

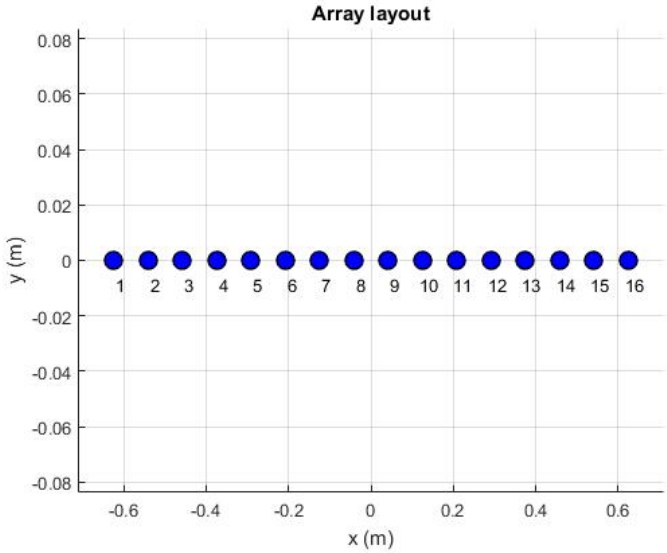

Figure 3.2 - 16 antenna unidimensional array layout

Being x_n the position of the *n*th dipole along the x-axis, the *n*th displacement phase factor is:

$$e^{j\boldsymbol{kd}_n} = e^{j2\Pi x_n \cos(\phi)\sin(\Theta)}. \tag{3.6}$$

Let **a**=$[a_0, a_1, \dots, a_n]$ be the array coefficients, where a_i=1 with *i*=0,1,2,…,*n*. Therefore, we may express the array factor as

$$A(\Theta, \phi) = \sum_{n=1}^{16} a_n e^{j2\Pi x_n \cos(\phi)\sin(\Theta)}, \tag{3.7}$$

and the dipole gain, by

$$G(\Theta, \phi) = \left|\frac{\cos(0.5\Pi\cos(\Theta)}{\sin(\Theta)}\right|^2. \tag{3.8}$$

At the horizontal plane, $\Theta = 90°$ (xy-plane), the array factor will be:

$$A(\phi) = \sum_{n=1}^{16} a_n e^{j2\Pi x_n \cos(\phi)}, \tag{3.9}$$

and the azimuthal power pattern, represented in figure 3.3, can be given by

$$G_{tot}(\phi) = |A(\phi)|^2 G(\phi) = \left| \sum_{n=1}^{16} a_n e^{j2\Pi x_n \cos(\phi)} \right|^2 \times 1. \tag{3.10}$$

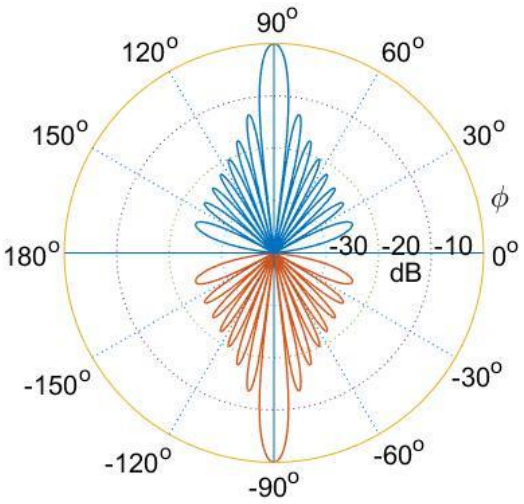

(a)

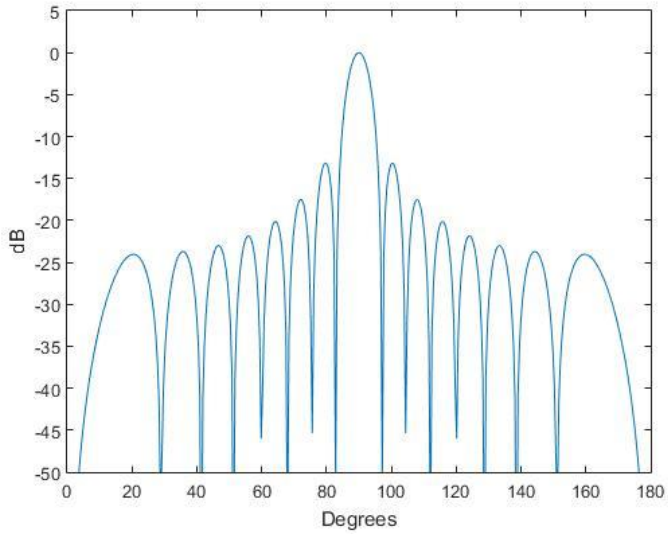

(b)

Figure 3.3 - Azimuthal power pattern for 16 dipole array with $\frac{\lambda}{2}$ spacing and uniform weight coefficients, in polar (a) and rectangular (b) coordinates

According to figure 3.3, the first side lobes on either side of the main peak (at ϕ=90°) are approximately 13 dB down. It's possible to reduce and force zero side love levels by controlling the array coefficients **a** and the distance **d**.

As it can be seen from (3.4), the main factors influencing the array pattern are the feed coefficients **a**, the inter-element spacing **d** and the array geometry. Half wavelength uniform element spacing was chosen based on two main criteria, the mutual coupling effect and the grating lobes effect. Mutual coupling is the phenomenon of currents developed in each antenna that do not depend only on own excitement, but have contributions from other elements of the array. The smaller the element spacing, stronger will be the effect. In transmitting antenna arrays, the mutual coupling effect renders the array pattern multiplication property (3.3) inapplicable, as it results in similar elements having different patterns [38]. Figure 3.4 shows an example of mutual impedance between two dipole antennas working at 1.8 GHz in order to their spacing.

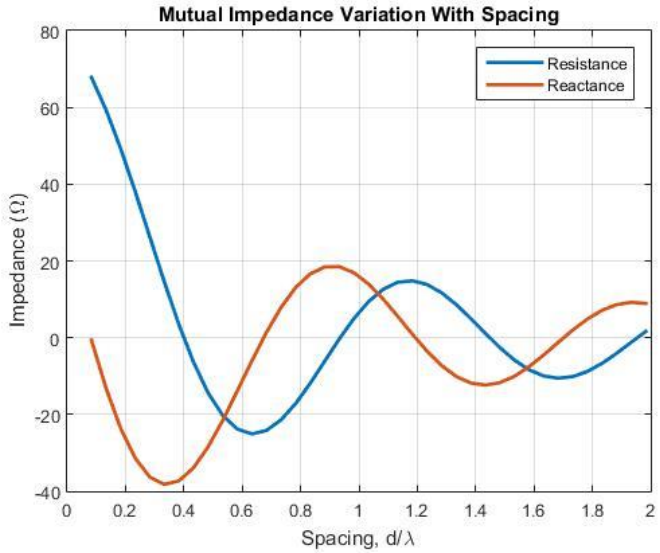

Figure 3.4- Mutual impedance of two dipoles according to spacing in λ units

As expected, the further apart the antennas are, the less mutual coupling is observed. However, for higher **d** (spacing) values, undesirable strong radiation beams, known as grating lobes, may appear. Figure 3.5 shows the presence of grating lobes at 48,15 and 131,8 degrees for uniform spacing of $d = \frac{3\lambda}{2}$.

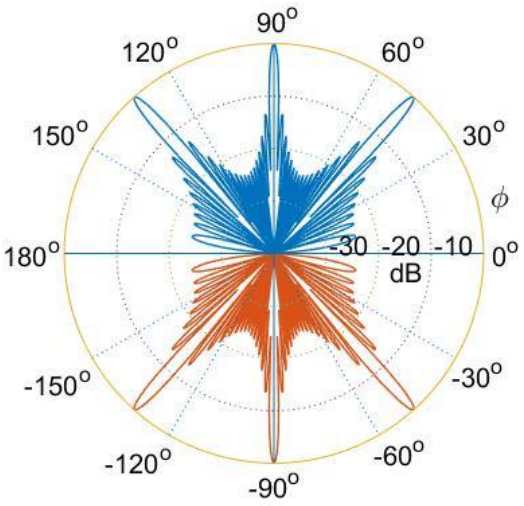

(a)

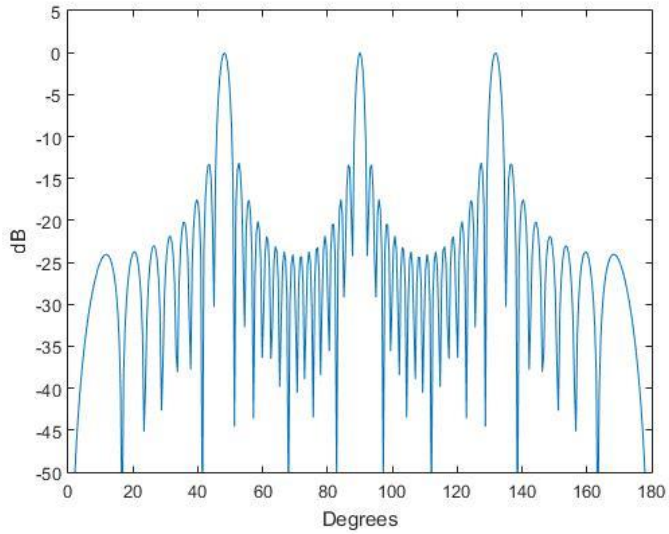

(b)

Figure 3.5 -Azimuthal power pattern for 16 dipole array with $\frac{3\lambda}{2}$spacing and uniform weight coefficients, in polar (a) and rectangular (b) coordinates

For a spacing of $d = \frac{3\lambda}{4}$ and uniform weights coefficients results the pattern shown in figure 3.6.

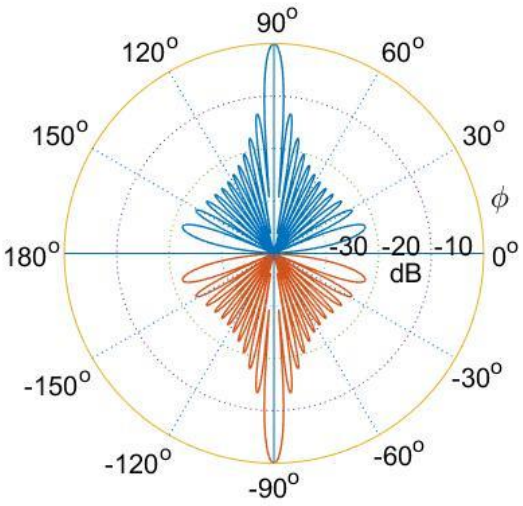

(a)

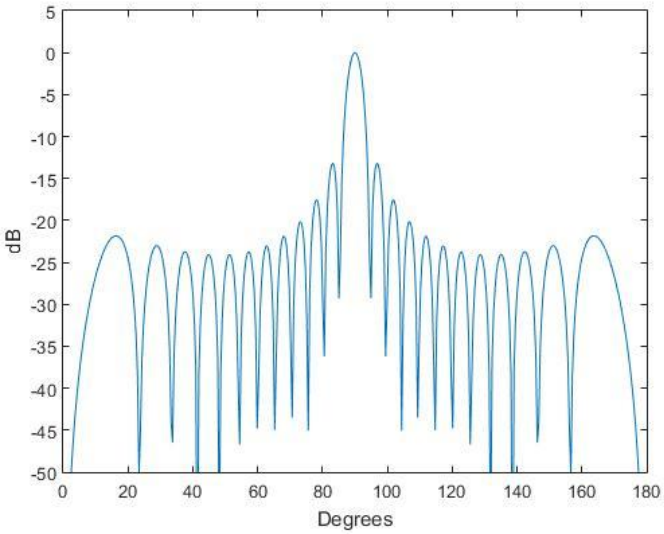

(b)

Figure 3.6 -Azimuthal power pattern for 16 dipole array with $\frac{3\lambda}{4}$spacing and uniform weight coefficients, in polar (a) and linear (b) coordinates

Compared to $\frac{\lambda}{2}$ spacing, the $\frac{3\lambda}{4}$ spacing seems to yield better results, however, if we introduce phased weight coefficients given by:

$$w_n = a_n e^{-j2\Pi x_n dcos(\phi_0)}. \quad (3.11)$$

Rearranging (3.9), results for the array factor the following expression

$$A(\phi) = \sum_{n=1}^{16} w_n e^{j2\Pi x_n \cos(\phi)}, \tag{3.12}$$

which is equivalent to write

$$A(\phi) = \sum_{n=1}^{16} a_n e^{j2\Pi x_n (\cos(\phi) - \cos(\phi_0))}, \tag{3.13}$$

By employing this method, the array can be steered to ϕ_0. With current $d = \frac{3\lambda}{4}$ spacing, for steering angles of 65 degrees and lower, or 115 degrees and higher, there are grating lobes in the visible space. This effect can be eliminated by decreasing the separation between array elements to $\frac{\lambda}{2}$ or less, where mutual coupling is stronger. Figure 3.7 shows this effect, for $\phi_0 = 45°$ and $d = \frac{3\lambda}{4}$.

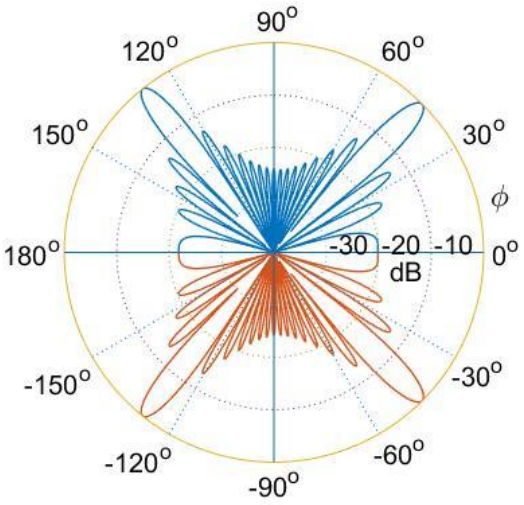

(a)

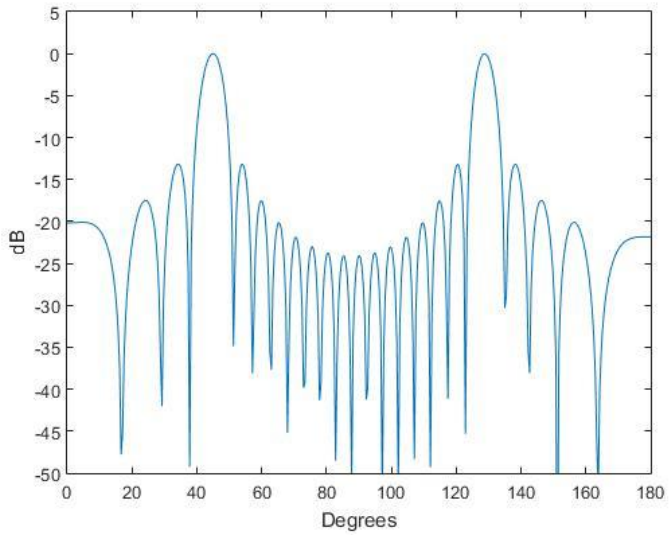

(b)

Figure 3.7 -Azimuthal power pattern for 16 dipole array with $\frac{3\lambda}{4}$ spacing steered to $\phi_0 = 45°$, in polar (a) and rectangular (b) coordinates

Studies for 32 and 64 elements arrays were also performed. From the simulations results of Table 3.I, becomes obvious that the number of antennas mainly impacts beamwidth, and the larger the array, the narrower will be the beam.

Table 3.I - Beamwidth for 16, 32 and 64 antenna arrays

Nr. of antenna elements	3dB beamwidth (degrees)
16	6.3455
32	3.1728
64	1.5864

3.3 Bi-dimensional antenna array

Taking the 16 element $\frac{\lambda}{2}$ spaced array as a starting point, it was replicated in parallel to form a bi-dimensional array with $N_v \times N_h$ antennas. Studied cases comprise arrays of $N_h = 16$ and $N_v = 4\ or\ 6$ elements.

Each array was spaced $d_y = \lambda$ with uniform weight coefficients. Note that each horizontal array has different weights, but along the same array the weights are uniform. Three azimuthal radiation patterns were calculated per bi-dimensional array with weight coefficients represented in tables 3.II and 3.III. The main goal of these simulations is to prove that despite different weightings for each horizontal array, the overall azimuthal radiation directivity remains unchanged. This weight coefficient permutation method introduced here will be the basis for the proposed constellation shaping technique addressed in Section 4.5 and Section 4.6.

Both array layouts are represented in figure 3.8.

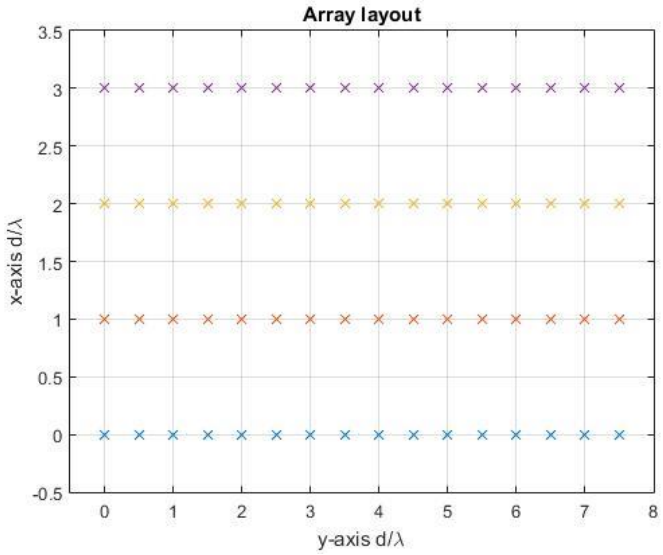

(a)

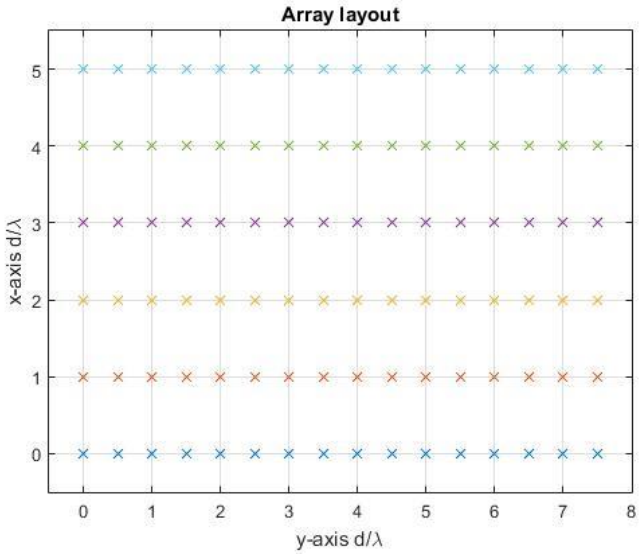

(b)

Figure 3.8 - 4x16 (a) and 6x16 (b) antenna bi-dimensional array layout

In case of a bi-dimensional array, all the previous equations remain valid in exception for the array factor, which now as to account for elements with two dimensional coordinates (x and y Cartesian coordinates). Rewriting (3.7), (3.8) and (3.9), we get

$$A(\Theta,\phi)=\sum_{n=1}^{64} a_n e^{j2\Pi \sin(\Theta)(x_n\cos(\phi)+y_n\sin(\phi))}. \tag{3.14}$$

Considering again the horizontal plane, $\Theta = 90°$ (xy-plane), the array factor will be:

$$A(\phi)=\sum_{n=1}^{64} a_n e^{j2\Pi(x_n\cos(\phi)+y_n\sin(\phi))}, \tag{3.15}$$

and the azimuthal power pattern, is given by

$$G_{tot}(\phi)=|A(\phi)|^2 G(\phi)=\left|\sum_{n=1}^{64} a_n e^{j2\Pi(x_n\cos(\phi)+y_n\sin(\phi))}\right|^2 \times 1. \tag{3.16}$$

The weighting method consists in random permutations of the coefficients represented in tables 3.II and 3.III, and corresponding simulation results are shown in figures 3.9 and 3.10. Calculations for these coefficients are made in section 4.5, using (4.26).

Table 3.II - Weight coefficients for the 4x16 array radiation pattern simulations

4x16 array	**Array weights**			
Weight coefficients	a_1 *to* a_{16}	a_{17} *to* a_{32}	a_{33} *to* a_{48}	a_{49} *to* a_{64}
First simulation, (a) in figure 3.9	1	2j	2	j
Second simulation, (b) in figure 3.9	j	2j	2	1
Third simulation, (c) in figure 3.9	j	1	2j	2

Table 3.III - Weight coefficients for the 6x16 array radiation pattern simulations

6x16 array	**Array weights**					
Weight coefficients	$a_1 \; to \; a_{16}$	$a_{17} \; to \; a_{32}$	$a_{33} \; to \; a_{48}$	$a_{49} \; to \; a_{64}$	$a_{65} \; to \; a_{80}$	$a_{81} \; to \; a_{96}$
First simulation, (a) in figure 3.10	2	1	2j	j	4	4j
Second simulation, (b) in figure 3.10	4	2	2j	j	1	4j
Third simulation, (c) in figure 3.10	4j	1	2	4	j	2j

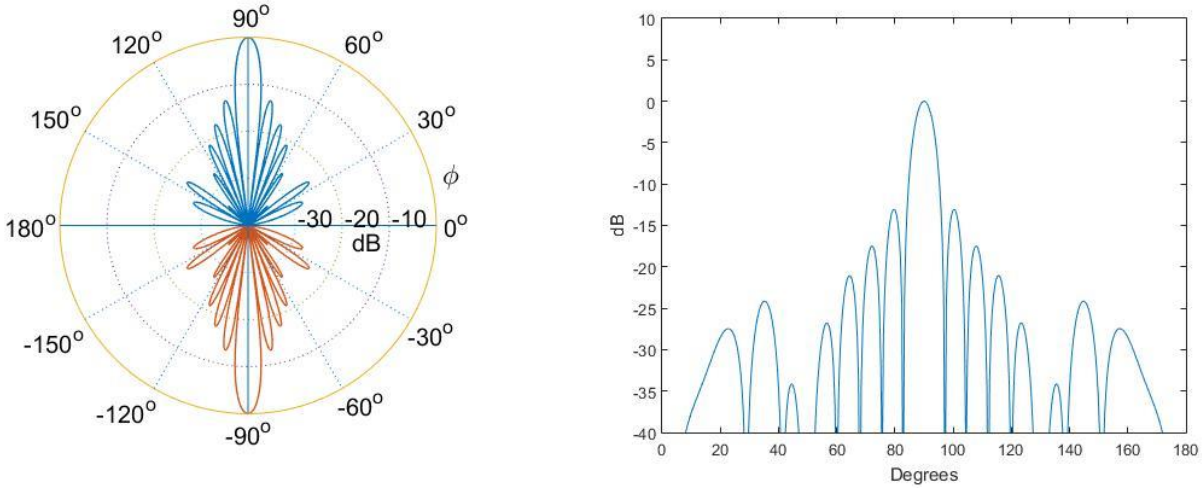

(a)

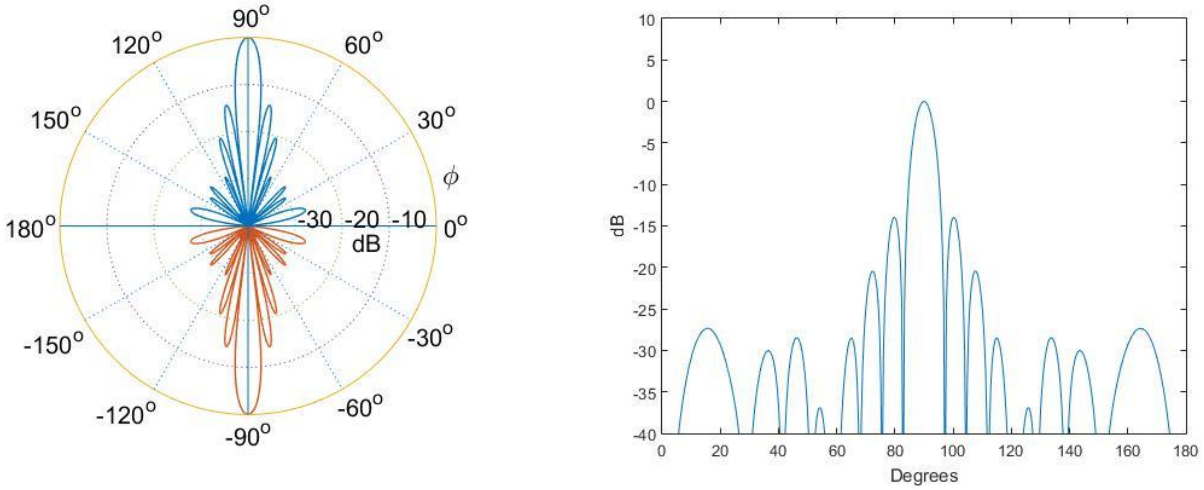

(b)

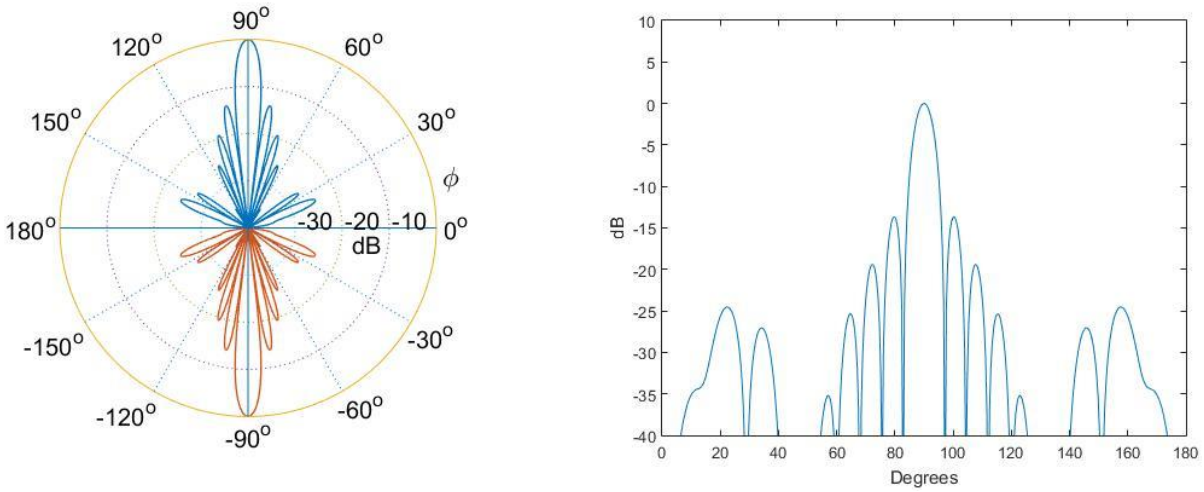

(c)

Figure 3.9 - Azimuthal power pattern for 4x16 dipole array with uniform weight coefficients per array

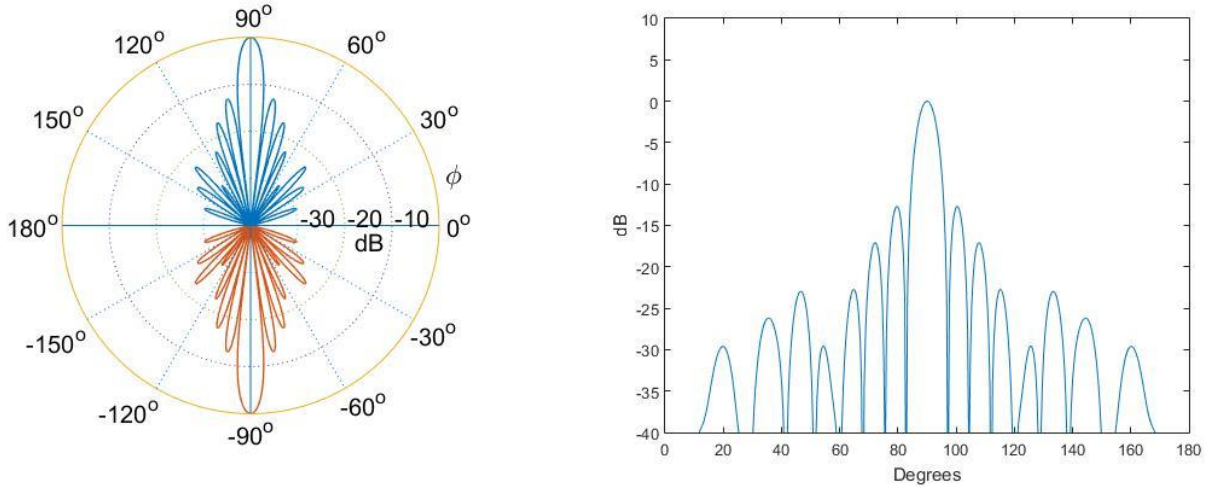

(a)

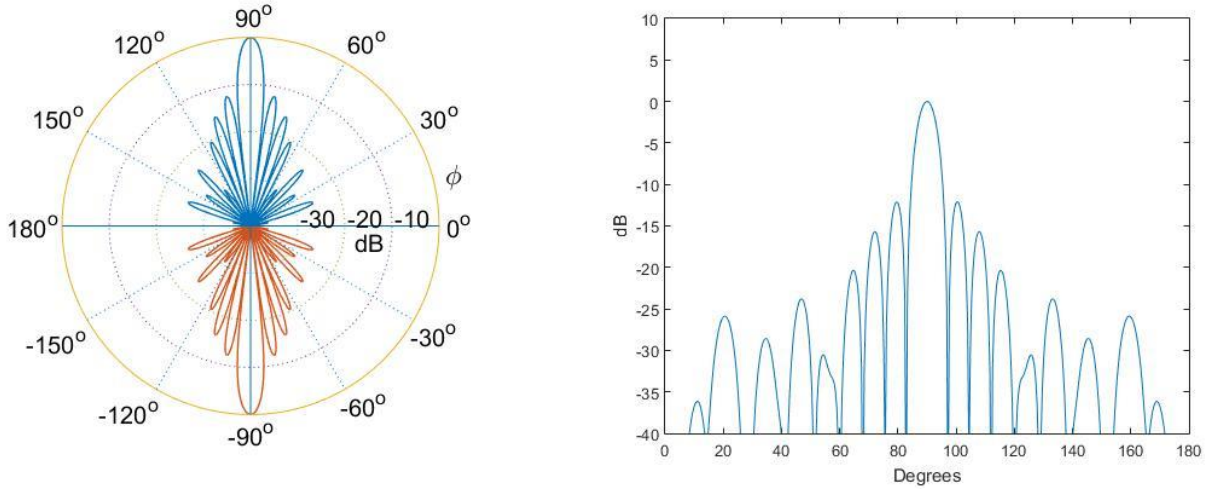

(b)

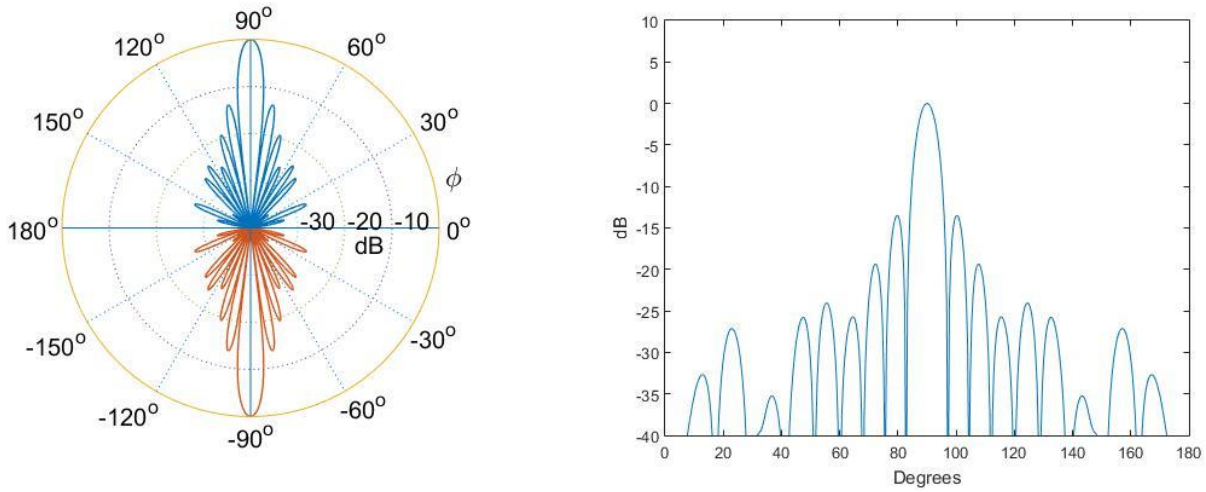

(c)

Figure 3.10 -Azimuthal power pattern for 6x16 dipole array with uniform weight coefficients per array

Comparing figure 3.3 with figures 3.9 and 3.10, it's possible to see that the array replication noticeably reduced side lobe level, while maintaining azimuthal directivity. Similar uniform spaced arrays of 8 x 16, 16 x 16, 16 x 32 and 16 x 64 antennas were also tested, but were considered impractical due to physical area constrains and elevated cost. Ideally, complete cancelation of side lobes is desirable, in order to ensure perfect beamforming and complete isolation.

Uniformly spaced antenna arrays are extensively studied in the literature. Most design methods employ heuristic optimization algorithms to find the optimum phase and magnitude values of excitation currents of the array elements [39] in order to optimize beamwidth and side lobe level, which means, despite increasing popularity of this type array, optimization still remains a challenging task [40]. The most commonly used methods for side lobe reduction involve some kind of amplitude tapering, in which the excitation current of array elements decreases with the distance from the center of the array. However, the main consequence of side lobe reduction is the broadening of the beamwidth. If the beamwidth is larger, the directivity of the array decreases, so a compromise between side lobe levels and beamwidth must be made. Thus, the main focus of array optimization for researchers is non-uniformly spaced arrays, as non-uniformly spaced arrays were not so extensively studied.

In 2008 a genetic algorithm combined with the conjugate gradient method was proposed by Oraizi and Fallahpour [41] in order to find the optimum antenna spacing for reduced side lobe level with truly remarkable results, achieving side lobe attenuations of -24.78 dB.

However, the iterative nature and lack of scalability of evolutionary algorithms make this approach too complex for larger arrays. That is, a linear increase in number of antenna elements usually causes an exponential increase in the search size and time. Since then, many optimization algorithms were proposed for the same purpose [39], [42], [43], still, the lack of scalability of all these techniques make them inapplicable and irrelevant in the context of this thesis.

Chapter IV takes the studied 4x16 and 6x16 antenna arrays and scrutinizes performance in a multiuser scenario without perfect beamforming. As mentioned in Section 2.2.3, to improve performance, a digital precoding was added to the above studied analog beamforming and the results from this hybrid beamforming approach can be seen at Section 4.4.

4 Chapter IV – Multilayer transmitter architecture

This chapter introduces a two layer massive MIMO transmitter scheme with beamforming gains to cope with propagation losses and supply a large number of co-channel users, with very high frequency reuse. In order to achieve high capacity and data rates, spectral efficiency must be enhanced by using large multilevel constellations that have high power requirements and high Peak-to-Average Power Ratio (PAPR), causing poor amplification efficiency.

By decomposing the transmitter structure into two tier layers, namely constellation shaping and beamforming, the proposed architecture can employ efficient nonlinear amplifiers combined with high spectral efficient QAM modulations, while maintaining capacity for a large number of co-channel users.

A brief outline of the chapter is as follows. Firstly, in Section 4.1, the Frequency-Domain Equalization method is described. Section 4.2 considers a system model based only spatial directivity, called layer 2 hereinafter. Section 4.3 studies inter user co-channel interference (CCI) and a Minimum Mean Square Error (MMSE) interference cancellation technique. Sections 4.4, 4.5 and 4.6 introduce and aggregate the constellation shaping method, denoted as layer 1 from now on, to the overall system model.

4.1 Single Carrier with Frequency Domain Equalization versus Orthogonal Frequency Division Multiplexing

OFDM is currently adopted and standardized in a wide range of wireless applications. The main virtue of this system is the resiliency to multipath propagation, providing a viable low complexity solution for ISI mitigation. Nonetheless, although OFDM has become a preferred choice for broadband communications, it still suffers from several drawbacks.

One of the major drawbacks of conventional OFDM schemes lies on their strong envelope fluctuation and, consequently, high PAPR, which implies amplification difficulties. A large PAPR would drive power amplifiers at the transmitter into saturation, producing interference among the subcarriers, degrading the Bit Error Rate (BER) performance and corrupting the signal spectrum [44]. To avoid amplifiers distortion, the PAPR of the signal may be reduced.

Various methods have been proposed to reduce PAPR. Some of these methods can be based on signal distortion techniques, such as clipping [45], multiple signaling [46][47][48], and coding techniques [44]. However, this is achieved at the expense of signal processing complexity at the transmitter's side and, ultimately, increased non-linear distortion effects. In fact, even when these techniques are used, the resulting envelop fluctuations are still higher than the corresponding SC schemes. This means that when a SC modulation is employed for the same constellation symbols, the envelop fluctuations of the transmitted signal will be lower, allowing the use of more efficient power amplifiers, which makes it a good choice for a highly power efficient transmitter structure. But as all things in life, nothing comes without a downside, as high rate SC systems are more susceptible to frequency selective fading and ISI.

A good alternative approach to cope with ISI effects is the combination of SC modulations with FDE, which has comparable complexity to OFDM while avoiding the above mentioned drawbacks associated with MC implementations [49]. To further improve performance, a nonlinear Decision Feedback Equalizer (DFE) can be used, as it can easily outperform a linear FDE [50] and has been proven one of the most popular channel equalization techniques [51]. The DFE is based on the principle that once the value of the current transmitted symbol is computed, it is possible to remove the ISI contribution of that symbol in future received symbols. With relative ease of implementation, DFEs can fully cancel ISI from linear dispersive channels without excessive noise enhancement [52].

These properties justify the adoption of a system based on a SC transmission scheme with an iterative equalization in the frequency domain (IB-DFE) [50], as explained in further detail in Section 4.1.1.

4.1.1 Iterative Block Decision Feedback Equalization receiver structure

In 2002, an Iterative Block DFE (IB-DFE) for SC transmission was proposed [50] with both feedforward and feedback filters implemented by Discrete Fourier Transforms (DFTs). This yields significant lower complexity than traditional DFEs. Figure 4.1depicts the IB-DFE receiver structure.

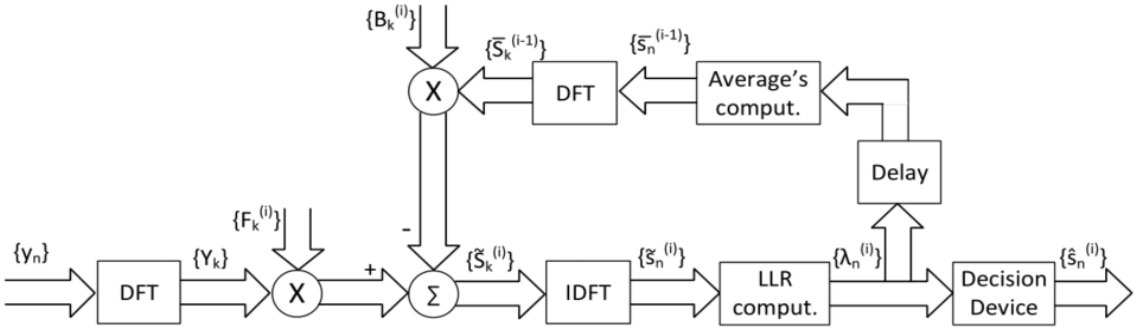

Figure 4.1 - IB-DFE receiver with soft decisions

The signal associated to a transmitted block is given by:

$$s(t) = \sum_{n=-N_G}^{N-1} s_n h_T(t - nT_S), \tag{4.1}$$

with T_S being the symbol duration, N_G the number of samples at the cyclic prefix, N denoting the useful samples of the block, $h_T(t)$ the pulse shape and s_n the *n*th transmitted symbol. As usual, the cyclic prefix corresponds to a periodic extension of the useful part of the block, i.e., $s_{-n} = s_{N-n}$ with higher length than the overall channel impulse response. At the receiver, these cyclic prefix samples are discarded to cancel inter block interference.

The corresponding block in the frequency domain is $\{Y_k; k = 0,1, \dots, N-1\} = DFT\{y_n; n = 0,1, \dots, N-1\}$, with:

$$Y_k = S_k H_k + z_k, \tag{4.2}$$

where H_k represents the channel frequency response for the *k*th subcarrier and z_k the corresponding Additive White Gaussian Noise (AWGN).

For a given *i*th iteration, the receiver output samples are given by:

$$\tilde{S}_k^{(i)} = F_k^{(i)} Y_k - B_k^{(i)} \hat{S}_k^{(i-1)}, \tag{4.3}$$

where $\left\{F_k^{(i)}; k = 0,1, \dots, N-1\right\}$ and $\left\{B_k^{(i)}; k = 0,1, \dots, N-1\right\}$ denote the feedforward and feedback equalizer coefficients, respectively. $\left\{\bar{S}_k^{(i-1)}; k = 0,1, \dots, N-1\right\}$ is the DFT of the soft decision block $\left\{\bar{s}_n^{(i-1)}; n = 0,1, \dots, N-1\right\}$, of the $(i-1)^{th}$ iteration, associated with the transmitted time-domain block $\{s_n; n = 0,1, \dots, N-1\}$.

The IB-DFE coefficients are chosen in order to maximize the SINR (Signal to Interference plus Noise Ratio) and are given by:

$$F_k^{(i)} = \frac{\kappa_F H_k^*}{\beta + [1 - (\rho^{(i-1)})^2]|H_k|^2}, \tag{4.4}$$

and

$$B_k^{(i)} = \rho^{(i-1)} F_k^{(i)} H_k - 1, \tag{4.5}$$

where $\beta = E[|N_k|^2]/E[|S_k|^2]$ and κ_F is selected to ensure that:

$$\sum_{k=0}^{N-1} F_k H_k / N = 1. \tag{4.6}$$

The correlation coefficient ρ, that is a measure of the reliability of the decisions used in the feedback loop, is given by:

$$\rho^{(i)} = \frac{E[s_n^* \hat{s}_n^{(i)}]}{E[|s_n|^2]}. \tag{4.7}$$

For now, the number of iterations used is restricted to one (although relevant for system overall performance, the number of iterations is not relevant for comparison purposes between the two layers, which is the main focus of this thesis), which means that $\rho = 0$, $B_k^{(0)} = 0$ and $F_k^{(0)}$ comes:

$$F_k^{(0)} = \frac{\kappa_F H_k^*}{\beta + |H_k|^2}. \tag{4.8}$$

Therefore, the IB-DFE reduces to a linear FDE.

4.2 Beamforming only (layer 2) system model and user interference

Assuming each $N_v \times N_h$ antenna array patch at the base station serves a single user with one receive antenna, the system model is represented in figure 4.2. For simplification purposes, only two users will be considered. Note that at this stage the same constellation symbol is used for all antennas, which means that no constellation shaping is employed and the transmitter only uses conventional beamforming.

Each base station array beamforming is optimized for the corresponding user azimuthal direction, which increases the SNR and the robustness against multiuser interference. It is clear, by analyzing figures 3.9 and 3.10, that the closer the users are, the greater will be the interference, as side lobe power reduces with the angular distance to the main beam. Figure 4.4 shows the BER for different angular distance values.

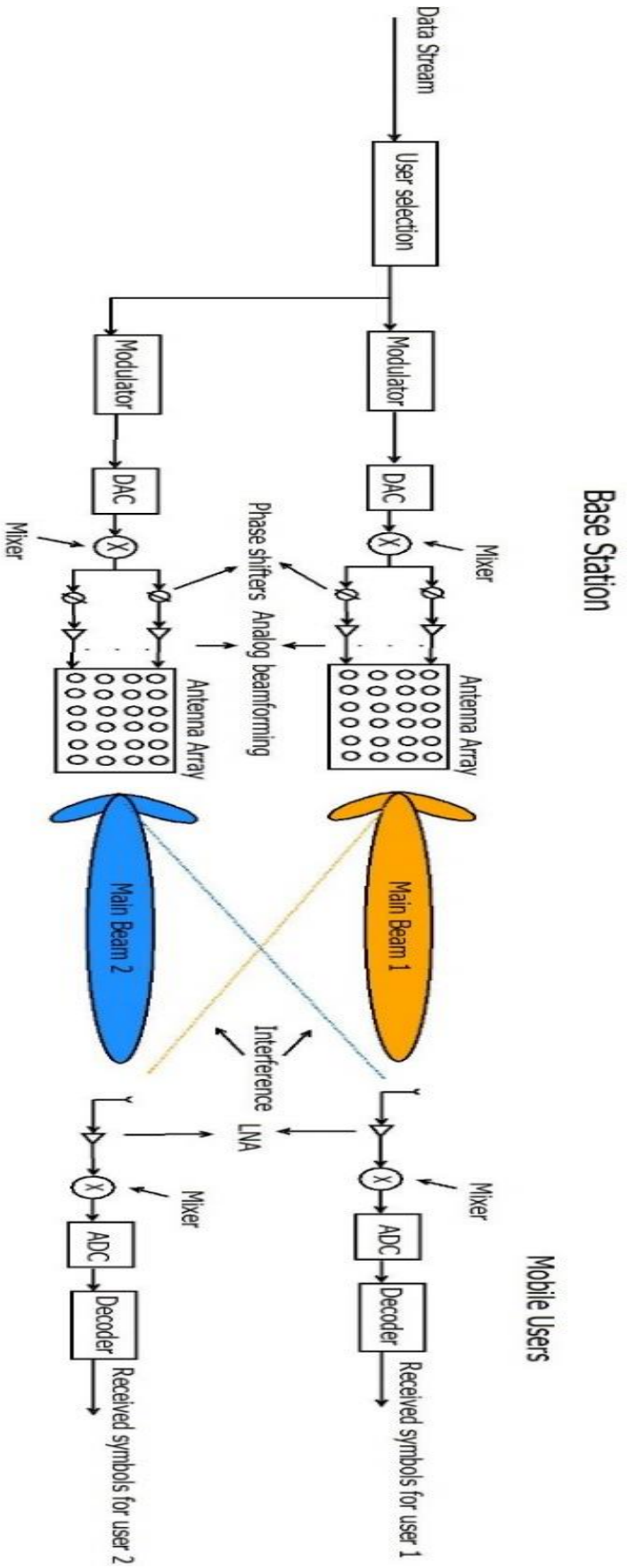

Figure 4.2 - Downlink system model with beamforming for two users

The angular distance (Θ) between users was determined from the maximum of the radiation pattern, see figure 4.3 for easier understanding.

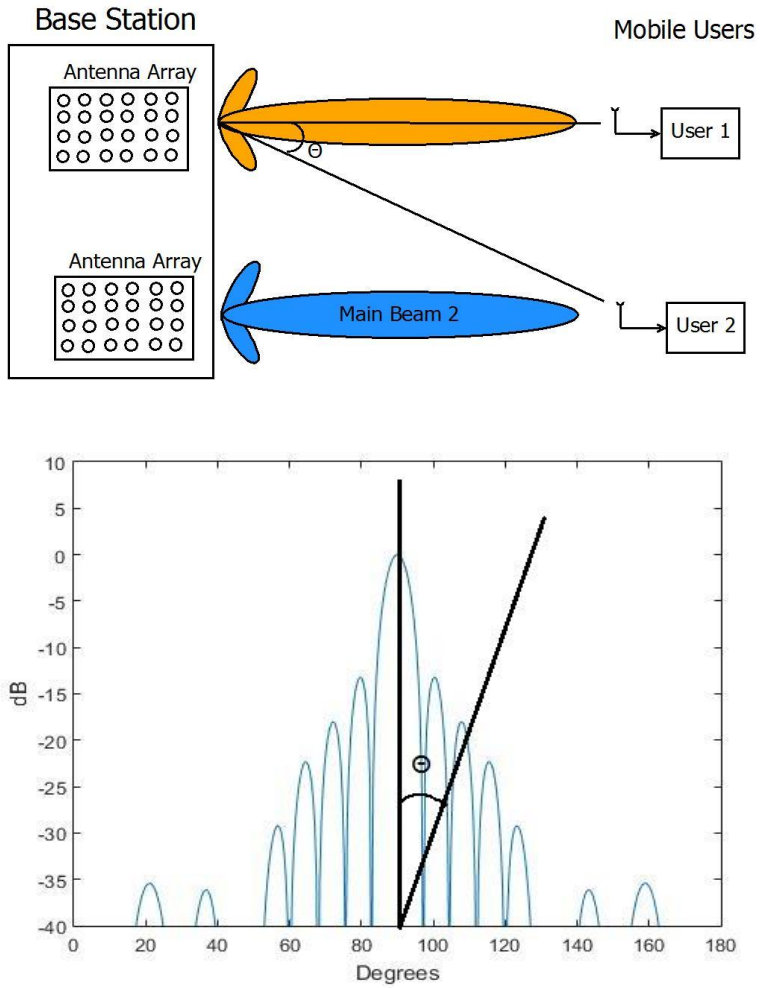

Figure 4.3 - Angular distance Θ between two users

The transmitted symbols s_n are selected randomly with equal probability from a M-QAM constellation (M=16 and M=64 were considered). Also, linear power amplification at the transmitter, perfect synchronization and perfect Channel State Information (CSI) are assumed. All the BER results are based on Monte Carlo simulations and expressed as function of $\frac{E_b}{N_0}$, where $N_0/2$ is the noise variance and E_b is the transmitted bit energy.

Also, a cluster channel model was considered. Each cluster is associated with a grouped set of multipath components with similar parameters. The energy reflected from these components leads to energy arriving at a different Angle of Arrival (AoA) or Angle of Departure (AoD), when viewed from the receiver or transmitter, respectively. Also, different path lengths lead to different time delays. For simplicity purposes, all AoAs are considered the same as the corresponding AoDs.

The used channel model is comprised of three clusters, each with four aggregated multipath components, each with its own AoD, power and delay. The first cluster AoDs are optimized according to the azimuthal radiation pattern maximum, which means 90º, the second and third clusters AoDs are directed randomly to simulate random reflections and refractions in multipath propagation.

The channel *h* impulse response is then given by:

$$h(\tau, \varphi_T) = \sum_{l=1}^{L} h_l\left(\tau_l, \varphi_{T,l}\right), \tag{4.9}$$

where τ_l is the delay and $\varphi_{R,l}$ is the azimuth AoD of the lth path and L is the total number of multipath components. The contribution of each multipath component is:

$$h_l\left(\tau_l, \varphi_{T,l}\right) = a_l e^{j\varphi_l} \delta(\tau - \tau_l) \delta\left(\varphi_T - \varphi_{T,l}\right), \tag{4.10}$$

where each multipath component has a complex amplitude $A_l = a_l e^{j\varphi_l}$, delay τ_l, and phase $\varphi_l = j2\pi\tau_l f_c$. Note that equations (4.9) and (4.10) give the directional impulse response of the channel h and only depict the contribution of each multipath component without any transmitter configurations.

Given the directional impulse response, the $1 \times M_T$ elements of **H** are designated as:

$$h_{1,n} = \sum_{l=1}^{L} h_l(\tau_l, \varphi_{T,l}) \times G_{tot}(\phi_l), \tag{4.11}$$

with $G_{tot}(\phi_l)$ given by (3.16) and $M_T = N_v \times N_h$ antenna elements. Also, all multipath components suffer Rayleigh fading and all **H** elements are fully correlated, which means the bi-dimensional array acts like a single huge antenna.

For user separation (Θ) values ranging from 2 to 20 degrees the following BERs were obtained (figure 4.4 and 4.5).

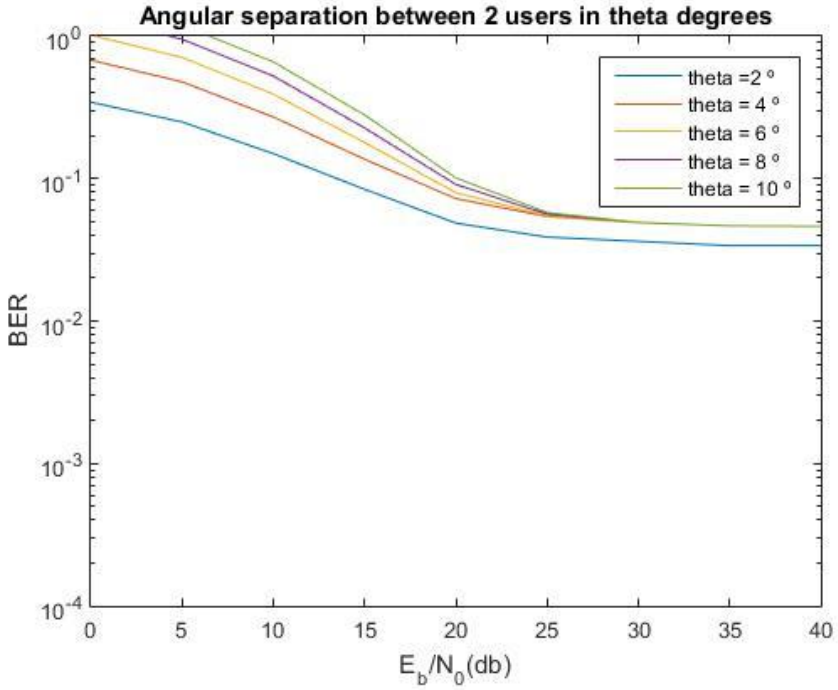

(a)

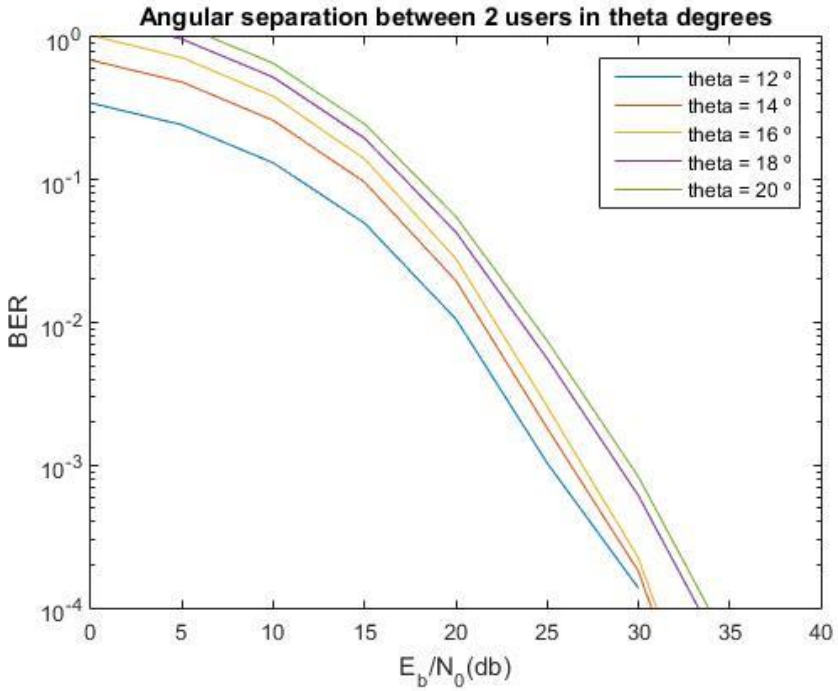

(b)

Figure 4.4 - BER for Θ ranging from 2 to 20 degrees (layer 2) for 16QAM. (a) considers 0 to 10 degrees. (b) considers 12 to 20 degrees

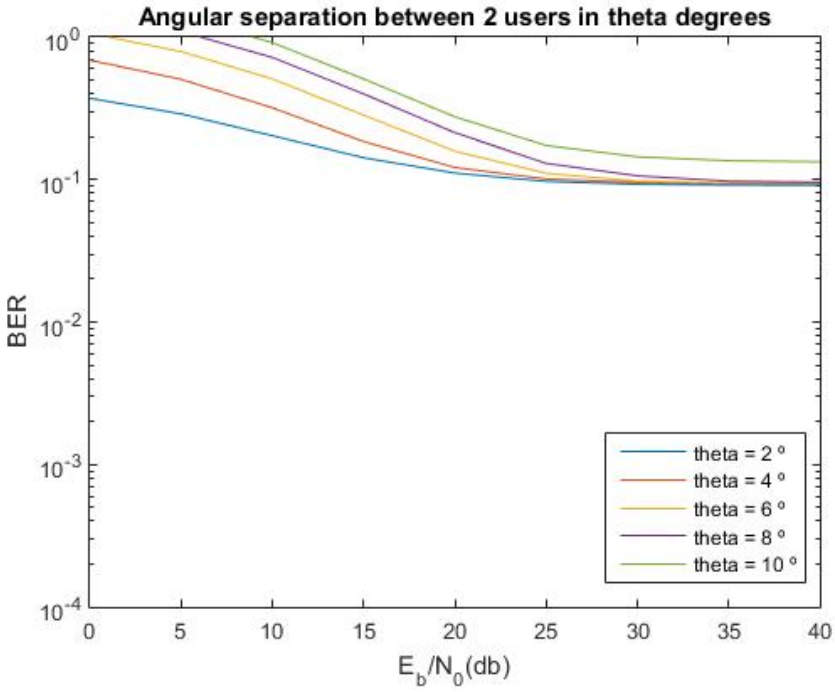

(a)

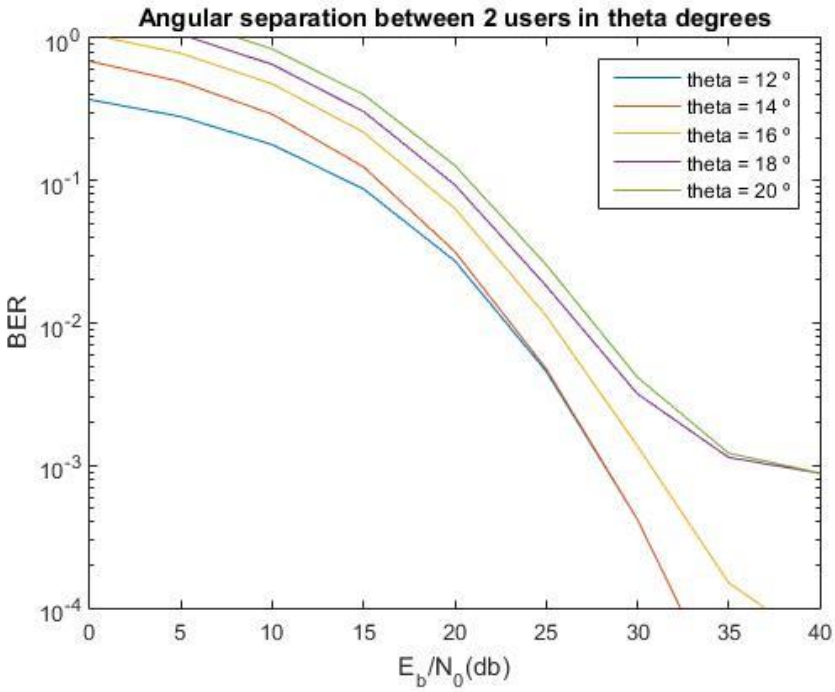

(b)

Figure 4.5 - BER for Θ ranging from 2 to 20 degrees (layer 2) for 64QAM. (a) considers 0 to 10 degrees. (b) considers 12 to 20 degrees

The poor system performance for 0 to 10 degrees can be explained by the occurrence of CCI from users that share the same frequency channel. Even though beamforming mitigates this effect for separation above 10 degrees, it's still not enough to guarantee reliable communication in realistic scenarios, in which users may be closer to each other. This co-channel interference can be handled using interference cancelation technology.

Having these problems in mind, next section analyses CCI and characterizes some interference cancellation techniques. Furthermore, a linear MMSE precoding algorithm is proposed.

4.3 Co-channel interference cancelation precoding

Co-channel interference is the phenomenon where the signal from two or more radio transmitters using the same frequency cause an undesired interference effect in each other. If one or more signals, besides the intended one, arrive at the receiver at the same frequency, the receiver is unable to separate and decode them properly, leading to a deterioration in performance.

In this section, precoding of the transmitted signals in MIMO systems is discussed. It should be noted that this type of processing at the transmitter requires perfect CSI at the transmitter. With CSI available at the transmitter, the transmitted symbols, either for single-user or multi-user can be somewhat separated by means of pre-equalization.

In point-to-point systems, precoding means that multiple data streams are emitted from the transmitter with independent weightings such that the throughput is maximized at the receiver. For the multi-user scenario the premise is the same, except the data streams are intended for different users. Precoding achieves this goal exploiting transmit diversity by means of weighting the data stream. Basically, the transmitter sends the coded data to the receiver using a pre-knowledge of the channel.

In multi-user MIMO systems, a multi-antenna transmitter simultaneously communicates with multiple receivers (each having one or more antennas). This is more commonly known as Space-Division Multiple Access (SDMA). Precoding algorithms for SDMA systems can be divided into two categories: linear and nonlinear. Although managing to achieve channel capacity [53], nonlinear algorithms are significantly more complex and linear techniques usually achieve reasonable performance with much lower complexity.

4.3.1 Linear precoding

Linear precoding implementations include Maximum Ratio Transmission (MRT) [54], Zero-Forcing (ZF) and Wiener (or linear MMSE) filtering [55].

Finding the optimal linear precoding is no easy task, as the precoding weights for a given user are selected to maximize the Signal-to-Noise-plus-Interference Ratio (SNIR). This means that precoding can be perceived as a way to find the optimal balance between enhancing signal gain while minimizing inter-user interference. In the approach to achieve such balance is where the techniques differ from each other.

MRT maximizes the signal gain at the intended user, which is close to optimal in noise-limited systems, where the inter-user interference is negligible when compared to the noise. ZF precoding works in the opposite way, aiming to nullify the inter-user interference at the expense of signal gain. ZF performance is close to optimal in interference-limited systems (negligible noise when compared to the interference) or when the system has a large number of users. A balance between MRT and ZF is the so-called MMSE filtering [55], which ponders between maximizing signal power and suppressing interference [56].

4.3.2 Nonlinear precoding

Nonlinear precoding is designed based on Costa's theorem of Dirty Paper Coding (DPC) [57], who imagined a partially covered paper with dirt indistinguishable from the ink marks made by the writer. The theorem states that if the writer knows where the dirt is, it can transmit as much information by writing on the paper as if it was clean, even though the reader has no idea where the dirt is. Transposing the theorem for wireless communications, the dirt is the interference, the paper is the channel, the writer is the transmitter and the reader is the receiver. Costa observed that any known interference at the transmitter can be cancelled without any power penalty if the optimal precoding scheme is applied to the transmitted signal. Several variations of DPC include Tomlison-Harashima (THP) precoding [58], [59] and the vector perturbation technique of Hochwald [60].

4.4 Proposed linear MMSE precoding

The system is composed by three main elements, namely the transmitter, the channel (H) and the receiver. Considering 2 $N_v \times N_h$ arrays for a total of M antennas at the base station and 2 users with single antenna, we have the system is shown in figure 4.6.

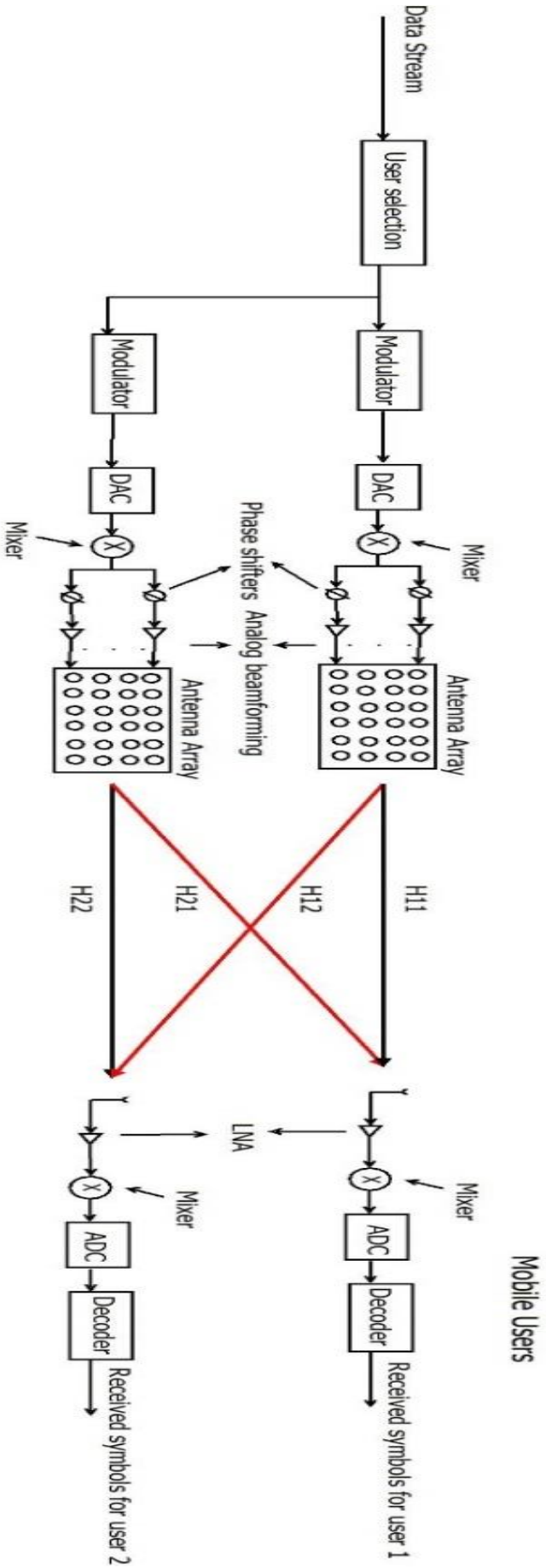

Figure 4.6 - Physical channel model

The channel with 2 outputs and 2 inputs is denoted as 2 x 2 matrix.

$$\boldsymbol{H} = \begin{bmatrix} \boldsymbol{H11} & \boldsymbol{H21} \\ \boldsymbol{H12} & \boldsymbol{H22} \end{bmatrix}, \tag{4.12}$$

which may be represented as

$$\boldsymbol{H} = \begin{bmatrix} h_{1,1} & \dots & h_{M,1} \\ h_{2,1} & \dots & h_{M,2} \end{bmatrix}, \tag{4.13}$$

where **H11**, **H12**, **H21** and **H22** are $1 \times {}^{M}/_{2}$ matrices where each entry $h_{i,j}$ denotes the attenuation and phase shift between the i^{th} transmitter antenna and the j^{th} receiver.

To understand the symbol interference, let's consider the received signal by user 1 in the first time slot, given by

$$y_1 = \boldsymbol{H11}x_1 + \boldsymbol{H21}x_2 + z_1, \tag{4.14}$$

and the received signal by user 2 given by:

$$y_2 = \boldsymbol{H12}x_1 + \boldsymbol{H22}x_2 + z_2, \tag{4.15}$$

with z_1 and z_2 being additive the AWGN on the first and second user's receiver, respectively.

Representing the above equation in matrix notation results in

$$\begin{bmatrix} y_1 \\ y_2 \end{bmatrix} = \begin{bmatrix} \boldsymbol{H11} & \boldsymbol{H21} \\ \boldsymbol{H12} & \boldsymbol{H22} \end{bmatrix} \begin{bmatrix} x_1 \\ x_2 \end{bmatrix} + \begin{bmatrix} z_1 \\ z_2 \end{bmatrix}, \tag{4.16}$$

or

$$y = \boldsymbol{H}x + z. \tag{4.17}$$

Assuming that the receiver knows **H** and y perfectly, to solve for x, we need to find a precoding matrix **W** which satisfies **WH**=**I**, with **I** denoting the identity matrix. This cancels out **H12** and **H21** (see figure 4.6). The MMSE detector that meets this requirement is given by:

$$\boldsymbol{W} = \beta \boldsymbol{H}^{-1}, \tag{4.18}$$

where β is a constant to meet the total transmitted power constraint after pre-equalization, characterized by:

$$\beta = \sqrt{\frac{2}{T(\boldsymbol{H}^{-1}(\boldsymbol{H}^{-1})^{H})}}, \tag{4.19}$$

Where *T* represents the trace operator, and

$$\boldsymbol{H}^{-1} = \boldsymbol{H}^{H}(\boldsymbol{H}\boldsymbol{H}^{H} + \frac{6_z^2}{6_x^2}\boldsymbol{I})^{-1}. \tag{4.20}$$

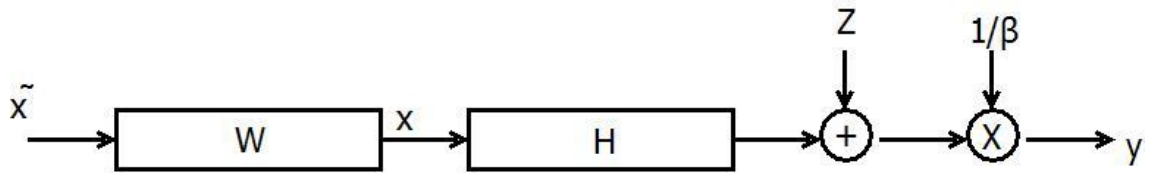

Figure 4.7 - Precoding and decoding structure

With precoding (figure 4.7), the transmitted signal by the BS is:

$$x = \sum_{k=1}^{2} W_k \tilde{x}_k\,, \tag{4.21}$$

where $\tilde{x}_k$ is the symbol to be transmitter to user k, W_k is the (M x 1) precoding vector for user k and z is AWGN noise.

Then, to compensate the effect of amplification by a factor of β at the transmitter, the received signal must be divided by β at the receiver, as shown in figure 4.7. For each user k, the received signal y_k will be

$$y_k = \frac{1}{\beta}(\boldsymbol{H}x + z) = \frac{1}{\beta}(\boldsymbol{H}\beta\boldsymbol{H}^{-1}\tilde{x}_k + z) = \tilde{x}_k + \frac{1}{\beta}z = \tilde{x}_k + \tilde{z}. \tag{4.22}$$

Figures 4.8 and 4.9 show the BER results for a scenario based on the previous testing conditions of Section 4.2, for an angular distance Θ with values ranging from 2 to 20 degrees between users, using 16QAM and 64QAM constellations. As intended, the inter-user interference is cancelled and results are satisfactory.

An interesting result is that for lower Θ values, the precoding scheme has better performance. These results support the idea that the system can offset the interference caused by beamforming when different users are very close to each other, even within same beamwidth. Another advantage of this precoding technique is that it allows the implementation of a low complexity receiver that doesn't have to perform channel matrix inversion operations, since the symbols are pre-equalized before transmission.

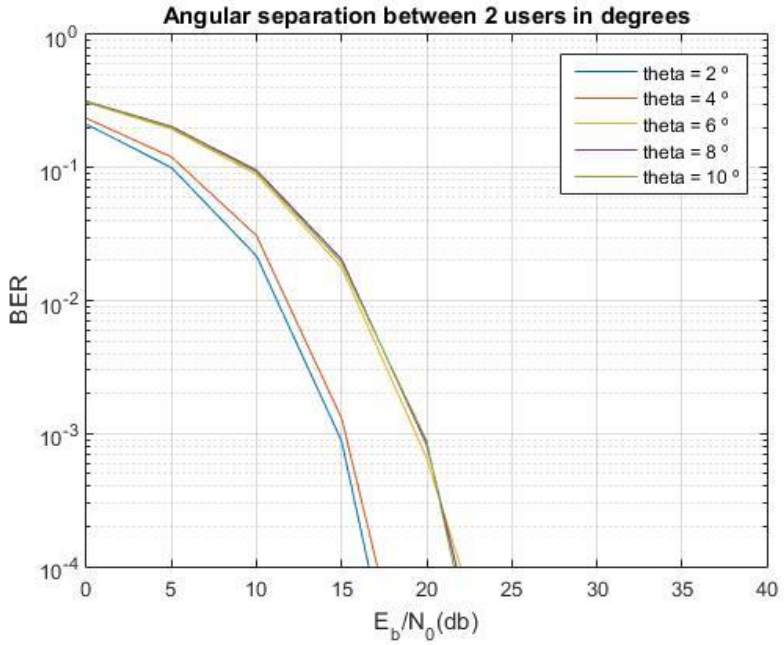

(a)

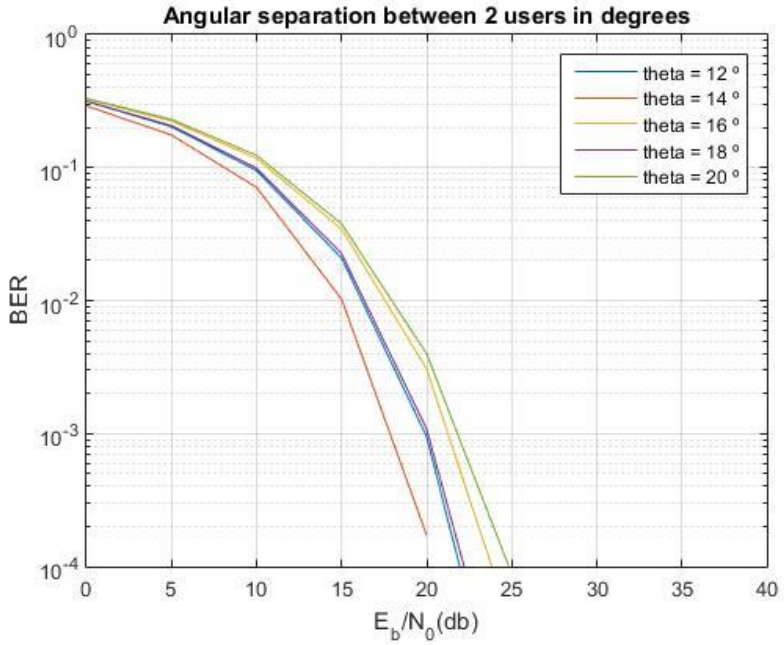

(b)

Figure 4.8 - BER for (Θ) from 2 to 20 degrees (layer 2) with MMSE precoding for 16QAM. (a) considers 0 to 10 degrees. (b) considers 12 to 20 degrees

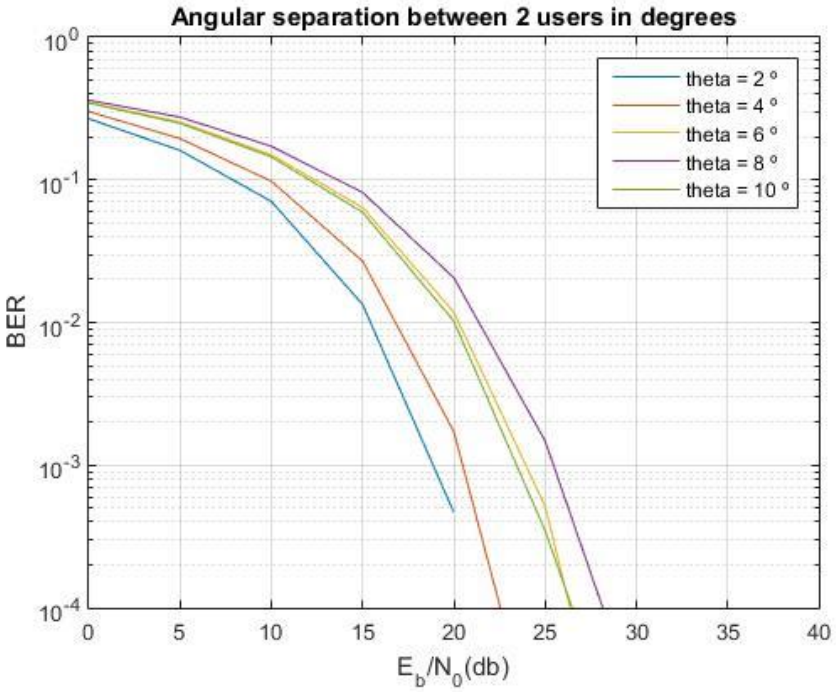

(a)

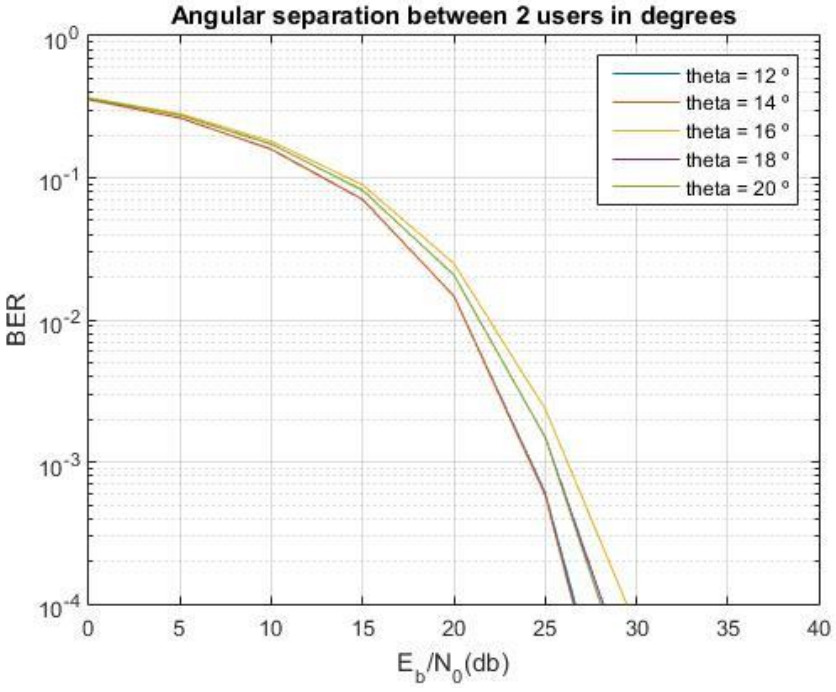

(b)

Figure 4.9 - BER for (Θ) from 2 to 20 degrees (layer 2) with MMSE precoding for 64QAM. (a) considers 0 to 10 degrees. (b) considers 12 to 20 degrees

A fairly straightforward technique to further improve the BER is the addition of more receive antennas per user, taking advantage of receive diversity with a Maximum Ratio Combining (MRC) or Selection Combining (SC) technique. Another option might be the implementation of a Successive Interference Cancellation (SIC) technique, or even a combination of both if the associated increase in complexity is not excessive.

Next section covers the constellation shaping method (layer 1) and presents some performance comparisons between both layers.

4.5 Constellation shaping

Multilevel modulations ensure high spectral efficiency but have high envelop fluctuations that impose restrictions on power amplification efficiency at the transmitter [5]. This problem can be surpassed by a transmitter structure where multilevel constellations are decomposed into several QPSK or OQPSK components, which in turn can be decomposed into quasi-constant envelope BPSK components.

The basic idea is to treat multilevel constellations as the sum of polar components associated to different BPSK signals with quasi-constant envelope that are amplified separately by nonlinear power amplifiers [61], [5]. Then, each BPSK component is transmitted by a different antenna array and the several components are combined at channel level to generate the original multilevel constellation amplified [5].

As shown by [61], any constellation symbol can be expressed as a function of the corresponding bits. Considering a constellation $S = \{s_0, s_1, \dots, s(N-1)\}$, with M points (i.e., $\#S = M$), where $s_n \in \mathbb{C}$. To each constellation symbol, a set of $\mu = \log_2 M$ bits $\beta = \left\{b_n^0, b_n^1, \dots, b_n^{(\mu-1)}\right\}$ in polar format are associated ($b_n^{(i)} = \mp 1 = 2\beta_n^{(i)} - 1, \beta_n^{(i)} = 0/1$). These sets of μ bits can be decomposed into $M = 2^\mu$ different subsets $\beta_m, m = 0,1, \dots, M-1$. With M points in constellation S and M different subsets of β_m, it's possible to write:

$$s_n = \sum_{m=0}^{M-1} g_m \prod_{b_n^{(i)} \epsilon \beta_m} b_n^{(i)}, n = 0,1, \dots, M-1. \tag{4.23}$$

For each s_n there is a system of M equations with M unknown variables g_m. With $(\gamma_{(\mu-1,m)}, \gamma_{(\mu-2,m)}, \dots, \gamma_{(1,m)}, \gamma_{(0,m)})$ being the binary representation of m with μ bits and defining β_m as the subset of bits where $b_n^{(i)}$ is included if and only $\gamma_{(i,m)}$ is 1, we may rewrite (4.23) as

$$s_n = \sum_{m=0}^{M-1} g_m \prod_{i=0}^{\mu-1} (b_n^{(i)})^{\gamma(i,m)}. \tag{4.24}$$

Since we have M constellation symbols in S and M complex coefficients g_m, writing (4.24) in matrix format results

$$\boldsymbol{s} = \boldsymbol{W}\boldsymbol{g}, \tag{4.25}$$

where $\boldsymbol{s} = [s_0 s_1 \dots s_{M-1}]^T$ denotes the ordered constellation, $\boldsymbol{g} = [g_0 g_1 \dots g_{M-1}]^T$ represents the ordered set of amplifiers gains and $\boldsymbol{W}$ is an appropriate Hadamard matrix. Since $\boldsymbol{s}$ is the Hadamard transform of $\boldsymbol{g}$, we can obtain $\boldsymbol{g}$ from the inverse Hadamard transform using

$$\boldsymbol{g} = \boldsymbol{W}^{-1}\boldsymbol{s}. \tag{4.26}$$

From (4.26) we can conclude that any M-ary constellation can be written as the sum of M BPSK sub-constellations. However, as power efficient constellations have no amplitude offset ($g_0 = 0$), only $M - 1$ BPSK signals are needed at maximum.

As example, we may consider the following 16-QAM with Gray mapping shown in figure 4.10.

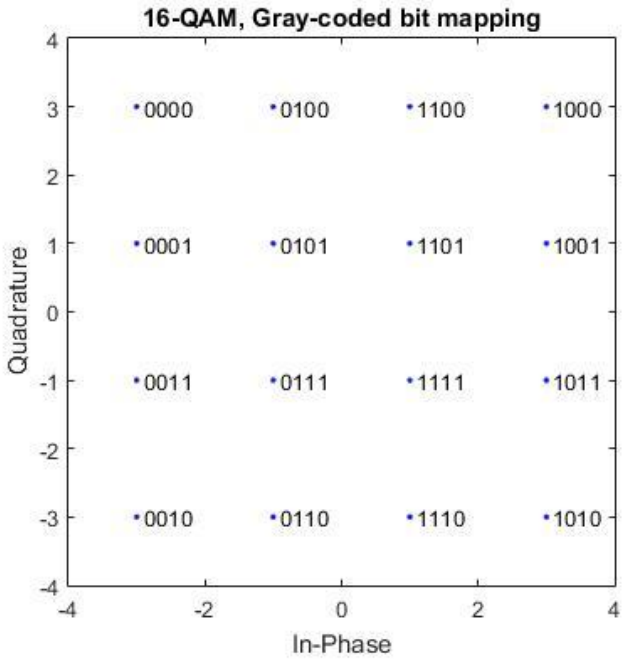

Figure 4.10 - 16-Gray mapping 16-QAM constellation

By using (4.26), the $\boldsymbol{g}$ coefficients associated to this constellation are

$$\boldsymbol{g} = \begin{bmatrix} 0.0625 & \cdots & 0.0625 \\ \vdots & \ddots & \vdots \\ 0.0625 & \cdots & 0.0625 \end{bmatrix} \begin{bmatrix} 3-3j \\ 1-3j \\ -1-3j \\ -3-3j \\ 3-j \\ 1-j \\ -1-j \\ -3-j \\ 3+j \\ 1+j \\ -1+j \\ -3+j \\ 3+3j \\ 1+3j \\ -1+3j \\ -3+3j \end{bmatrix} = \begin{bmatrix} 0 \\ 0 \\ 2j \\ j \\ 0 \\ 0 \\ 0 \\ 0 \\ 2 \\ 0 \\ 0 \\ 0 \\ 1 \\ 0 \\ 0 \\ 0 \end{bmatrix}.$$

The above calculations show that for 16-QAM constellations with Gray mapping, only $\log_2 M$ BPSK signals are needed, since the remaining g_m coefficients are zero. This conclusion can easily be extended to all M-QAM constellations with Gray mapping.

4.6 Proposed structure (Layer 1 + Layer 2)

Taking the $N_v \times N_h$ antenna structure, $N_v = \log_2 M$ amplification branches are used in parallel, namely $N_v = 4$ and $N_v = 6$ for 16QAM and 64QAM modulations, respectively. Each amplification branch is connected to $N_h = 16$ antennas. All but the first N_h antenna elements are employed to define directive beams for spatial multiplexing purposes and/or interference management (layer 2) (see sections 4.2 and 4.4). The first antenna element (marked as blue in figure 4.11) of each array is responsible for the constellation shaping (layer 1), as seen in figure 4.11.

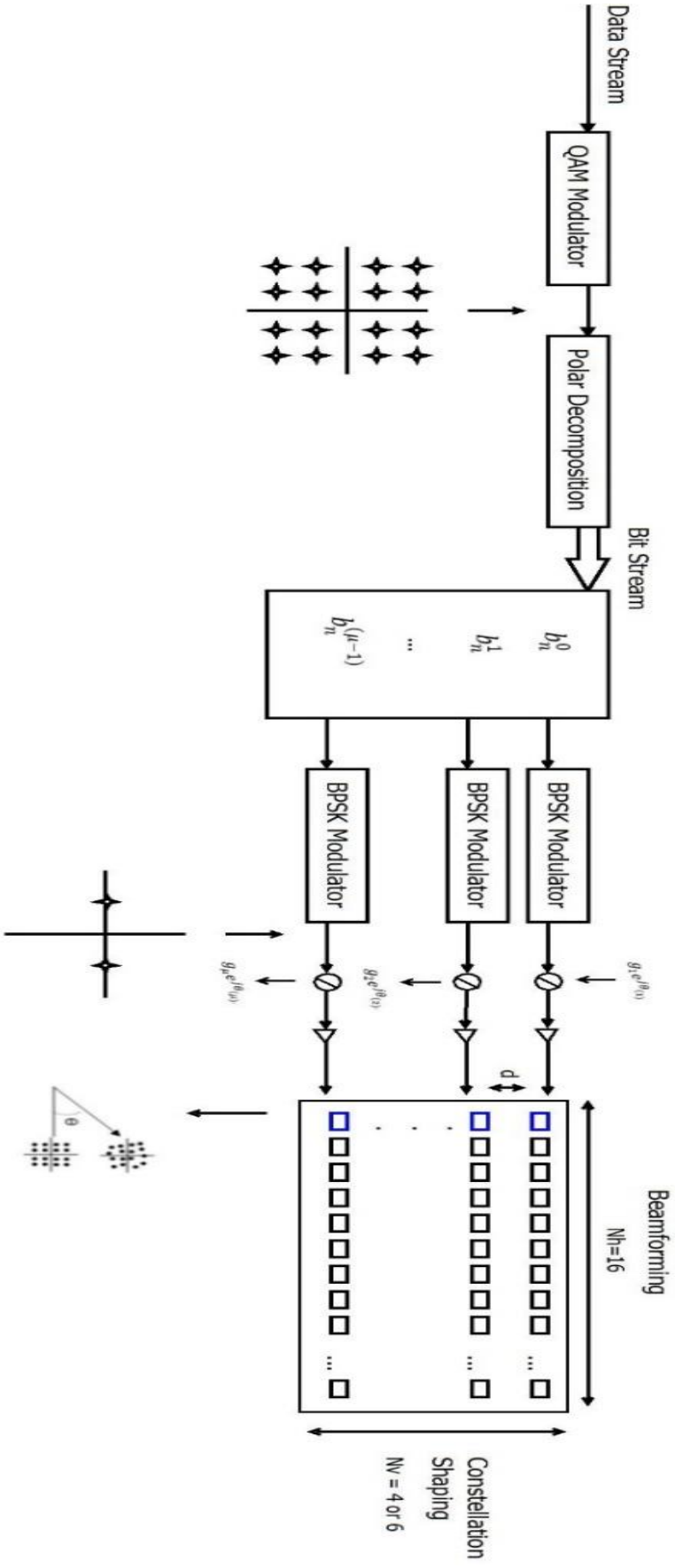

Figure 4.11 - Proposed multilayer transmitter structure

The transmitter architecture consists in N_v sets of N_h antennas. Each set has its own RF chain and guarantees efficient amplification by polar decomposition of larger QAM modulations. Each RF chain is associated to a BPSK component that is combined at channel level to generate the desired QAM modulation.

On top of efficient power amplification, if a phase shift or a non-uniform weight coefficient is introduced in each array, it is possible to steer the constellation shape to a specific angle ϕ. This creates directivity at the information level, as the constellation shaping is modified according to ϕ. So, a sequence of bits is converted into symbols while the shaping of the constellation is performed using a set of coefficients g_i with $i = 1, \dots N_v$, associated to every BPSK component. If for each user, the g_i coefficients are known only to the transmitter and the intended receiver, a new level of security is achieved at the physical layer, due to shaping.

It is important to note that each array transmits uncorrelated signals and phase variations between RF branches only affects the BPSK components that generate the constellation (layer 1) and doesn't affect the azimuthal radiation pattern. Under these conditions, the constellation symbols are shaped according to a direction ϕ, directly dependent on phase variations between the several amplification branches. Accordingly, this introduced directivity at the constellation level can be controlled by inducing specific phase rotations and/or weight coefficient permutations between RF branches. Then, this "altered" constellation is transmitted by the bi-dimensional antenna array studied previously, with azimuthal radiation directivity (layer 2).

4.6.1 Structure configuration

The considered arrangement of BPSK components along the N_v RF branches for 16-QAM and 64-QAM can be any permutation of the values present in table *4.I* and *4.II* (Same coefficients of tables *3.II* and *3.*III). Different coefficient arrangements result in different constellation shapes.

Table 4.I -g_i arrangements for 16-QAM

16-QAM	**RF branch order**			
	1	2	3	4
g_i coefficients	2j	1	2	j

Table 4.II - g_i arrangements for 64-QAM

64-QAM	**RF branch order**					
	1	2	3	4	5	6
g_i coefficients	2j	1	2	j	4j	4

For a proper reception, the receiver not only needs to be in the direction of the maximum radiated power, but also needs to know the constellation coefficients g_i and transmission direction ϕ, otherwise it receives a degenerated signal. Therefore, this transmitter achieves an additional security scheme inherent to the constellation mapping, as transmitted bits are converted into symbols of the constellation adapted by the g_i coefficients and ϕ, only known by the intended receiver. So, unauthorized users, unaware of the constellation parameters of layer 1 (g_i coefficients and ϕ) are unable to properly decode the information. Consequently, an additional layer of security is added, since any non-authorized receiver must estimate the g_i coefficients and array phase configuration used by the transmitter to compensate the phase rotations and distortion, caused by each amplification branch, affecting the received constellation.

To summarize, a M-QAM constellation can be decomposed as a sum of $\log_2 M$ uncorrelated polar components, defined by a set of nonzero g_i coefficients. These uncorrelated polar components are modulated as $\log_2 M$ BPSK signals with quasi-constant envelope components that are separately amplified by N_v nonlinear amplifiers and posteriorly transmitted by N_h antennas. Since these components are uncorrelated, directivity is only introduced at information level due to constellation shaping [62], done by a set of g_i coefficients. Additionally, variations of g_i's magnitude and phase shapes the constellation according to the angle ϕ, in which the constellation is optimized.

To assess the influence of the transmission direction on the constellation shaping security degree, the mutual information (MI) behavior was calculated as a function of ϕ.

4.6.2 Mutual Information

The MI of two random variables determines the mutual dependence between them. Basically, it quantifies the amount of information we can extract about one random variable, through the other. High MI indicates a large reduction in uncertainty about one random variable given the knowledge of another. Low MI indicates small reduction in uncertainty and zero MI means the two random variables are independent.

Formally, the MI of two discrete random variables X and Y whose joint probability distribution is $P_{XY}(x,y)$, can be defined as [63]:

$$I(X;Y) = \sum_{x,y} P_{XY}(x,y) \times \log\left(\frac{P_{XY}(x,y)}{P_X(x)P_Y(y)}\right) = E_{P_{XY}} \times \log(\frac{P_{XY}}{P_X P_Y}), \quad (4.27)$$

where $P_X(x)$ and $P_Y(y)$ are the marginal probability functions of X and Y respectively.

$$P_X(x) = \sum_y P_{XY}(x,y), \quad (4.28)$$

and

$$P_Y(y) = \sum_x P_{XY}(x,y), \quad (4.29)$$

with $E_{P_{XY}}$ being the expected value over the distribution *P*.

Mutual Information has several advantages over other similarity measures like the Euclidian distance. Besides being able to capture non-linear relations between variables, MI is not sensitive to scaling, so non normalized variables can be compared. Also, MI is robust towards noise and missing values in data.

Assuming discrete and equally probable symbols, s_n and s'_n, defined in a M sized constellation $\mathfrak{G}$, the Mutual Information between the input and the output of a communications system channel gives a measure of capacity of that channel, and can be given by [64]:

$$I(S;Y) = \log_2 M - \frac{1}{M}\sum_{s\in\mathfrak{G}} E_n\left[\log_2\left(\sum_{s'_n\in\mathfrak{G}} \exp(-\frac{1}{N_0}\left|\sqrt{E_s}(s_n - s'_n) + n\right|^2 - |n|^2\right)\right], \quad (4.30)$$

where $\boldsymbol{E_n}$is the expected value and E_s is the symbol energy.

An evolution of the MI considering the distortion effect in constellations caused by ϕ, between 0º and 360º was computed for a reference M-QAM (M=16 and 64) constellation. For the calculation of MI, s_n symbols are selected with equal probability from 16-QAM and 64-QAM constellations and it is considered an AWGN channel. Also, it is assumed a linear amplification at the transmitter and perfect synchronization at the receiver. MI results are based on Monte Carlo simulations and presented in function of the transmission angle ϕ for a fixed SNR value of 18 dB.

Figure 4.12 shows the MI evolution according to the constellation shaping angle ϕ.

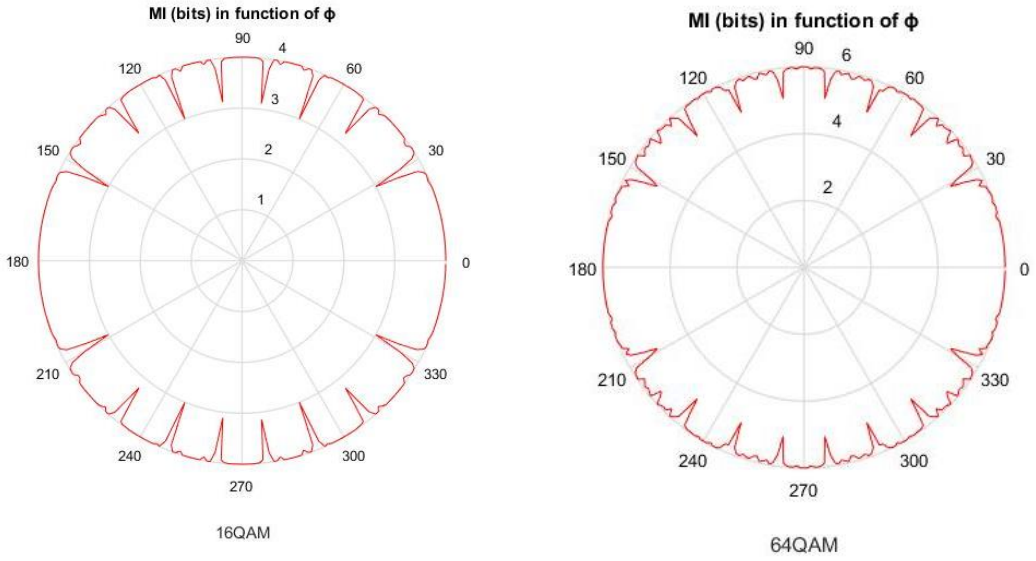

Figure 4.12 - MI evolution with ϕ for the authorized user for 16QAM (left) and 64QAM (right)

For both modulations, some ϕ angles show a decrease of MI which means a loss of one bit of information per symbol. Obviously, these angles should be avoided. Nonetheless, most directions ϕ can be used with unaffected MI, which enables successful decoding. As expected, 64QAM is not as robust as 16QAM to distortion effects and has more MI variations.

To take full advantage of these MI variations, it should be possible to optimize constellations to angles in the vicinity of the minimums, i.e., 25-29º or 31-35º. Under these conditions, if for some reason an eavesdropper tries to estimate ϕ, albeit with a possible estimation error, it can enhance the impact of said error since it can lead to the MI minimums. For an example, if the authorized user has a constellation optimized to $\phi_a = 29^o$ and the eavesdropper ϕ_e estimation is given by $\phi_e = \widehat{\phi_a} + \Delta\phi$, if $\Delta\phi = 1^o$ then $\phi_e = 30^o$, which corresponds to a MI minimum and leads to an enhanced degradation, preventing successful decoding.

Although not considered for this thesis, a possible future work might be the analysis of the ϕ_e estimation and impact of estimation errors in overall performance.

4.6.3 Simulation results

Fully correlated channel

Regarding the transmitter configuration, two different options were considered for comparison purposes. In the first one, the transmitter configuration is based on the layered structure (layer 1 + layer 2) presented in Section 4.6, with the constellations optimized for 58º. The second option consists in a transmitter of beamforming only (layer 2), presented in Section 4.2. Hence, in the first option, constellation shaping is combined with the horizontal spatial directivity caused by each horizontal array of 16 antennas. In the second option, the same constellation symbol is transmitted by all antennas, optimizing only the horizontal directivity of the beam towards the intended user. In both options, the array configuration is the same and vertical spacing between antennas is λ. In the horizontal plane, antennas are spaced $\frac{\lambda}{2}$. As in Section 4.2, users have only one receive antenna and only two users are considered, and the applied channel model is the same. Also, the same MMSE interference cancellation method presented in Section 4.4 is applied. For the sake of simplicity, angular separation between users was restricted to $\Theta = 2^o$ and $\Theta = 10^o$.

The results of figure 4.13 show that both transmitter configurations have similar performances (degradation lower than 4 dB for $\Theta = 2^o$ for 16QAM, approximately 6 or 7 dB for 64QAM between BER values of 10^{-1} and 10^{-3}). This means that the power efficient transmitter with constellation shaping can be adopted without major sacrifices in system's performance. Directivity in the vertical plane was not considered, since it has insignificant influence on overall system's performance.

Figure 4.14 shows the distortion effect suffered by the transmitted constellations with constellation shaping for the same Layer 1 + Layer 2 (blue) and Layer 2 only (red) scenarios.

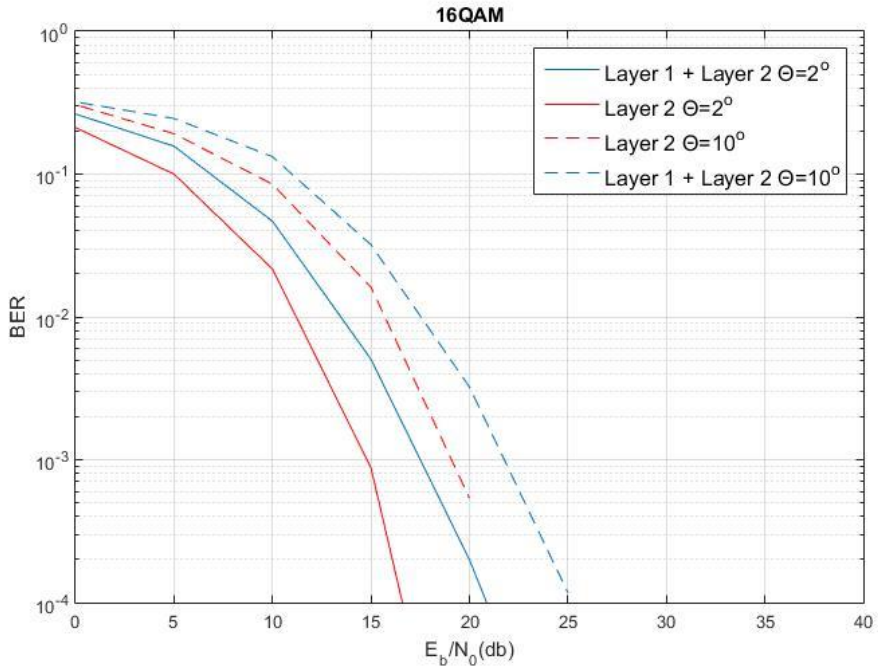

(a)

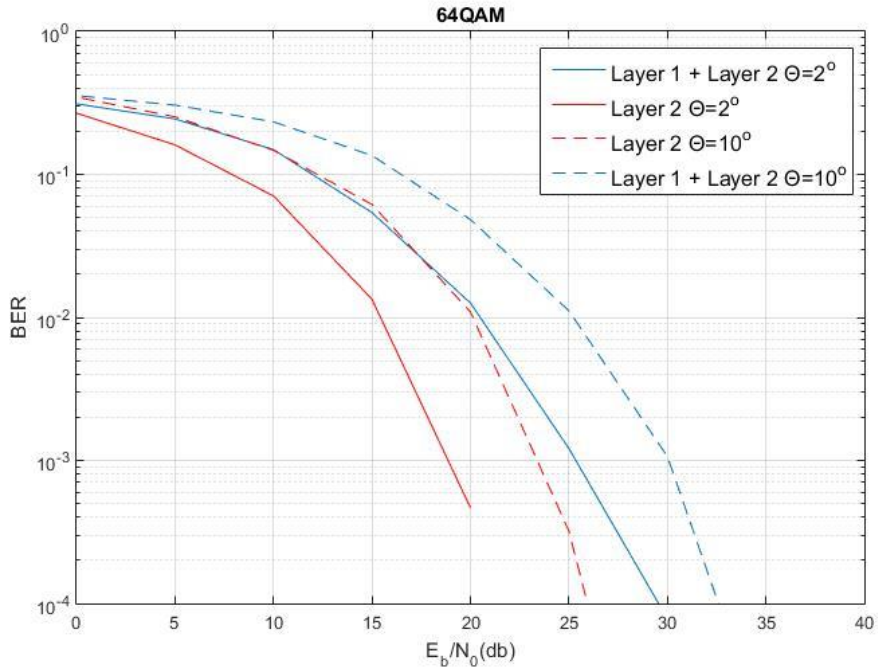

(b)

Figure 4.13 - BER performance for both configurations with MMSE precoding for 16QAM (a) and 64QAM (b)

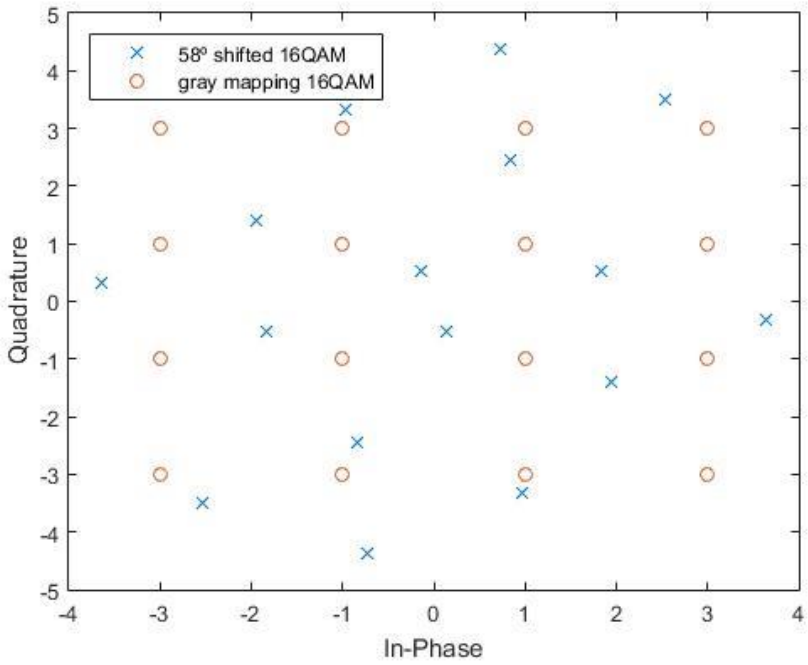

(a)

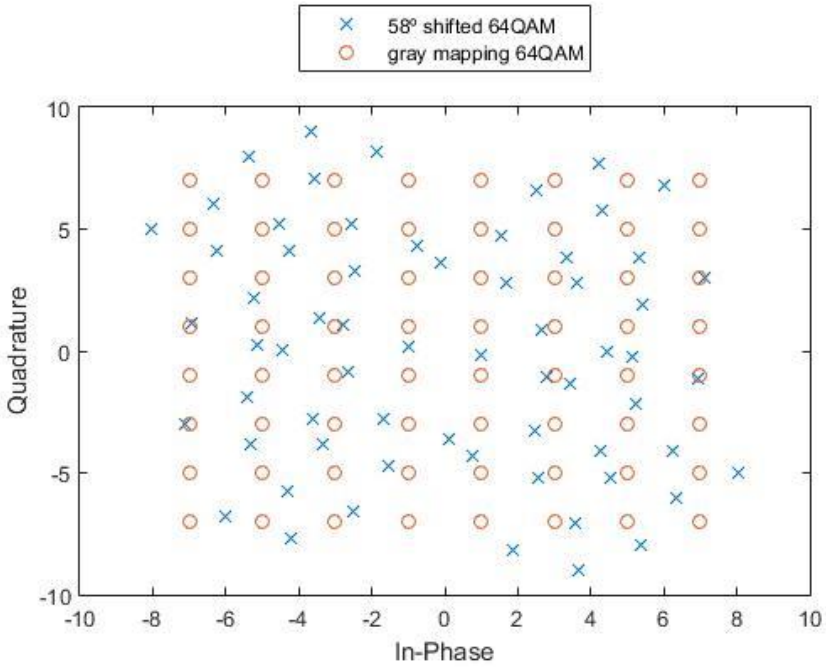

(b)

Figure 4.14 - Transmitted constellations for the Layer 1 + Layer 2 scenario (blue) and Layer 2 only (red), for 16QAM (a) and 64QAM (b)

It is clear that when the receiver has perfect knowledge of constellation coefficients $g_i$and transmission direction ϕ, it is able to successfully decode the transmitted information. In the case an eavesdropper tries to decode the information without knowing the transmission parameters, we obtain the performance results of figure 4.15. The 50% error rate allow us to conclude that the constellation shaping layer 1 can be extremely effective for physical layer security purposes, and this double layer architecture has similar performance of classical beamforming implementations, which use all antennas for directivity purposes. Note that figure 4.15 only presents simulation results for 16QAM, since results for 64QAM have an identical 50% error rate and don't add any more significant information.

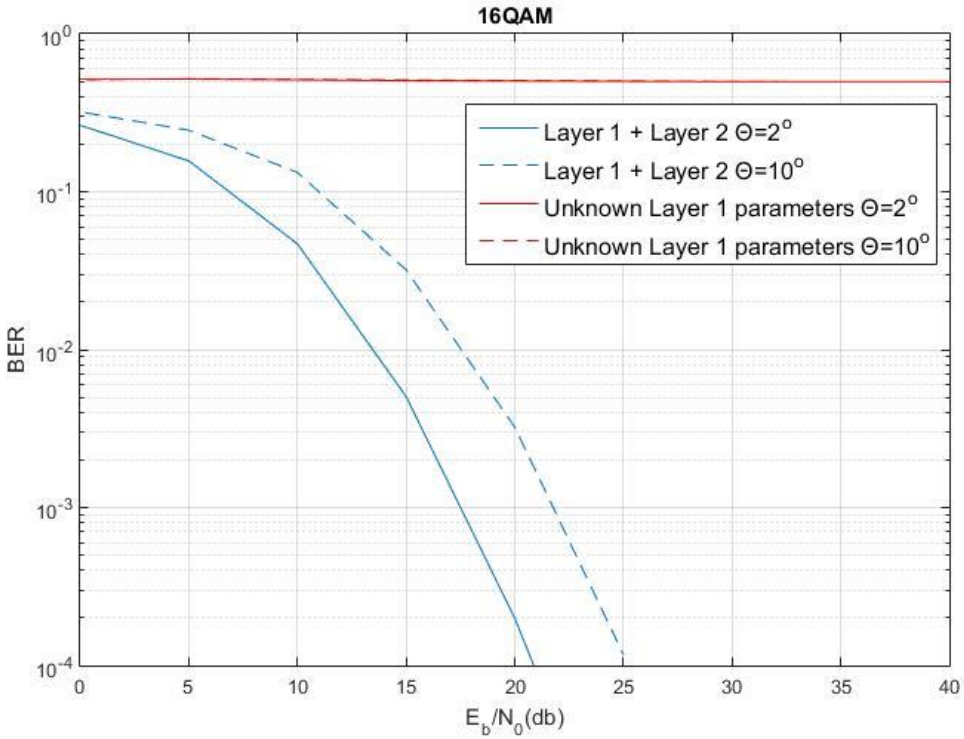

Figure 4.15 - Eavesdropper tries to decode degenerate constellation (50% error rate) for 16QAM

Uncorrelated channel between adjacent beamforming layers

Until now, all simulations considered all the channels fully correlated (as mentioned in section 4.2). However, it may be relevant to study the effect of channel correlation on overall system performance. Channel correlation is a measure of likeliness or dependence between multiple channels, and is mainly dependent on spatial correlation and antenna mutual coupling.

It is well known that short antenna spacing increases the spatial correlation and reduces capacity in multi antenna systems [65], [66]. As the studied system model considers a rich multipath scenario, the spatial correlation decreases by spreading the signal through several AoDs [67], and mutual coupling was already covered in section 3.2. It is convenient to recall that minimizing mutual coupling implies reducing the correlation coefficient between antenna elements.

As the system is being designed for the millimeter wave spectrum, a computation of the correlation coefficient (ρ) for a fixed antenna spacing of λ, from 1 to 50 Ghz using the S-Parameter characterization [68] is shown in figure 4.16.

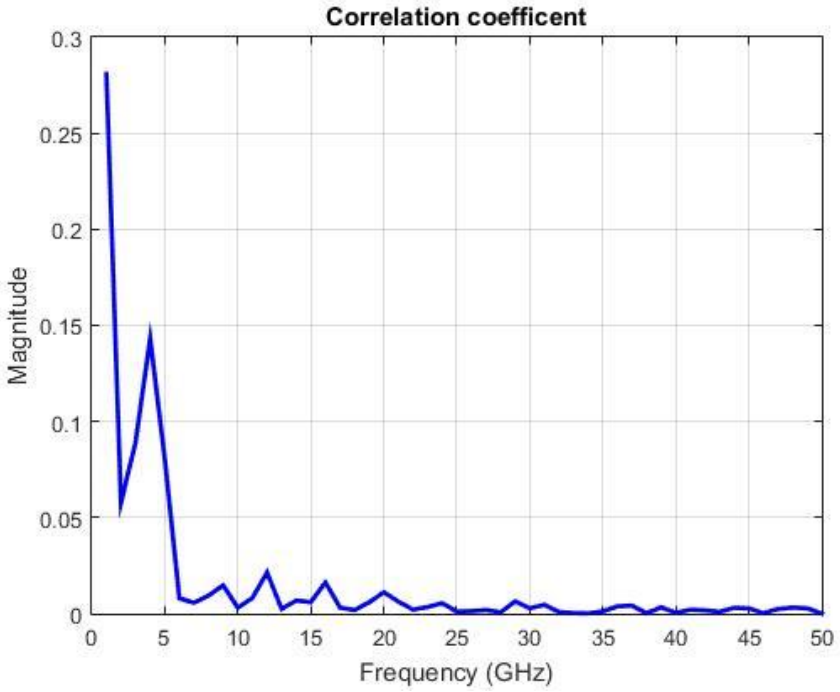

Figure 4.16 - Antenna correlation coefficient for a fixed spacing value of λ

Note that the spacing λ coincides with the spacing between each N_v beamforming layer.

The results of the previous figure allow us to conclude that there is only residual correlation between adjacent N_v layers for frequencies above 5 GHz. Considering this, it is not unrealistic to assume independent channels (ρ = 0) for each N_v beamforming layer. The BER for both layer configuration is the following (figure 4.17).

The results of figure 4.17 show at least a 3 dB improvement for both modulations for $\Theta = 2^o$ for 10^{-3} error rates. For $\Theta = 10^o$, improvements were in the order of 5-6 dB. These performance improvements are only dependent on the channel model and do not represent any additional computational complexity at both the transmitter or receiver.

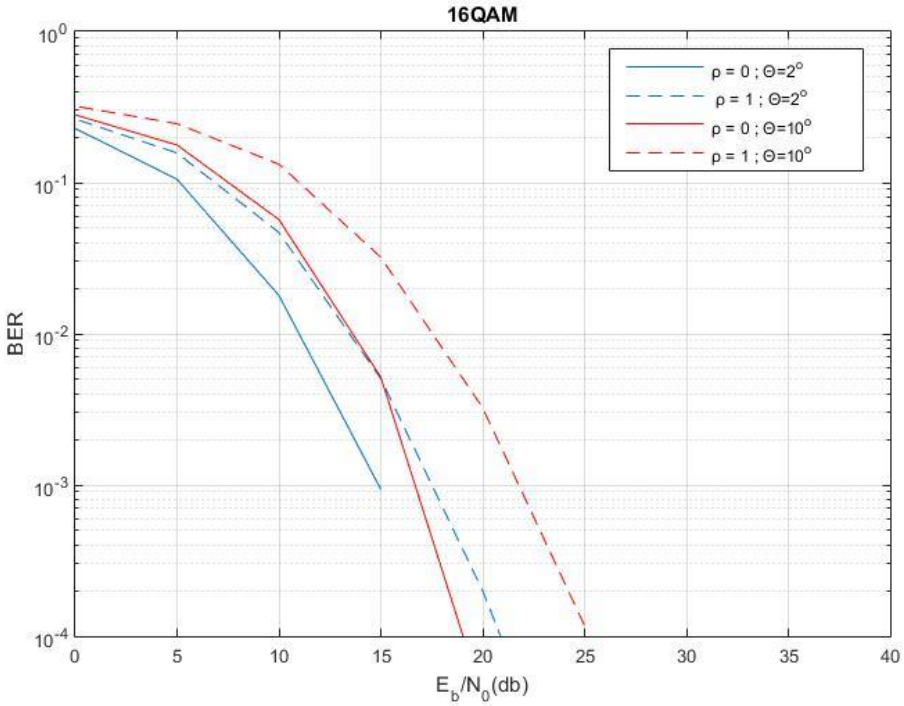

(a)

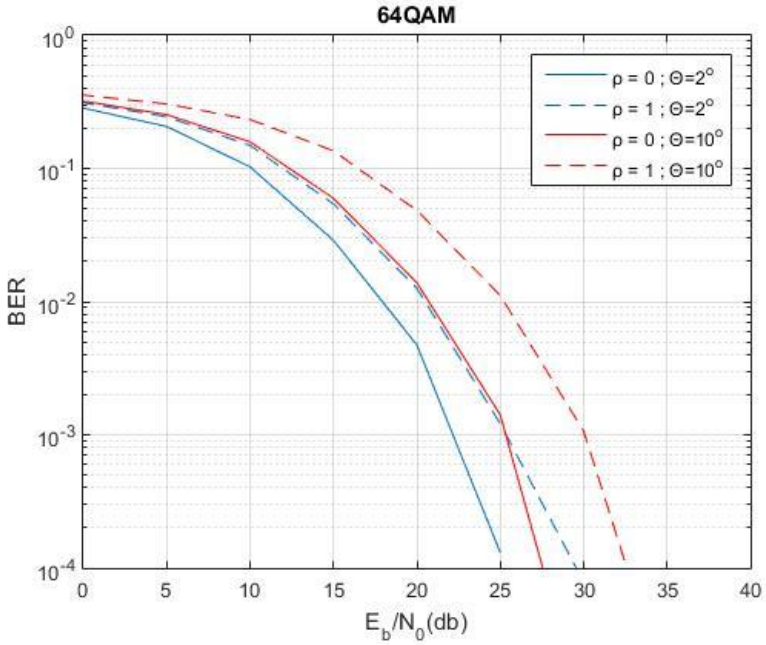

(b)

Figure 4.17 - BER performance for both ρ coefficients with MMSE precoding for 16QAM (a) and 64QAM (b)

Expanding the system for four users, for constellation mappings of $\phi_1 = 58^o, \phi_2 = 40^o, \phi_3 = 5^o$ and $\phi_4 = 90^o$ with ϕ_i denoting the optimization angle for the user i constellation, the BERs represented in figures 4.18 and 4.19 were obtained. Note that the same uncorrelated channel was assumed and these optimization angles were chosen based on the evolution of MI with ϕ (see figure 4.10). These particular angles ensure that there is no loss of information due to constellation shaping distortion.

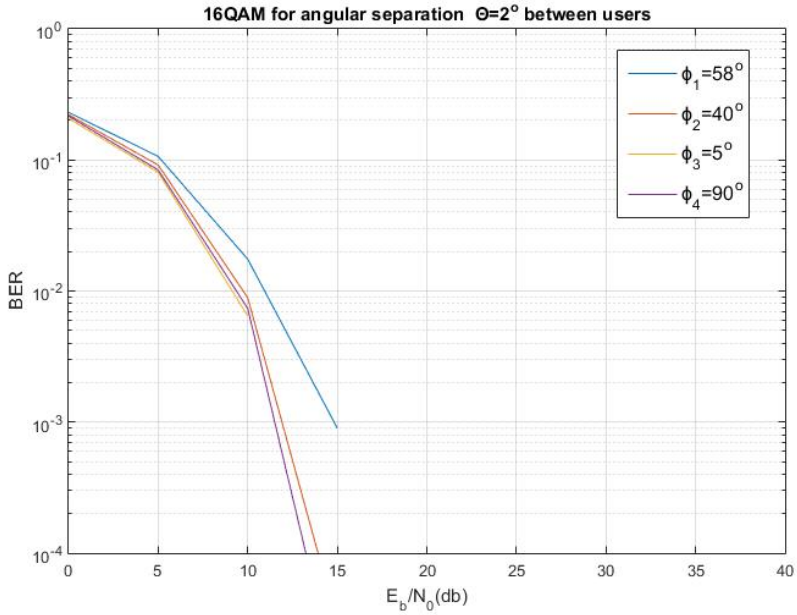

(a)

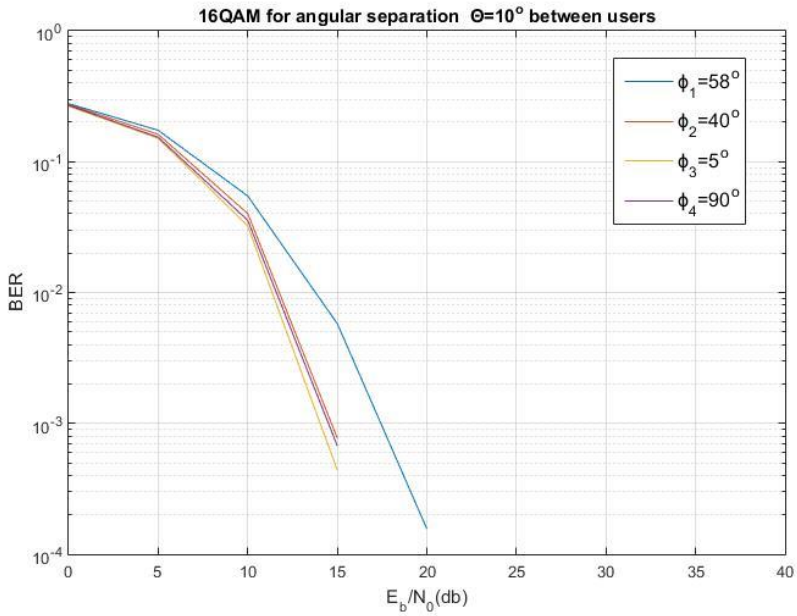

(b)

Figure 4.18 - System performance for 4 users for 16QAM for user separation $\Theta = 2^o$ (a) and $\Theta = 10^o$ (b)

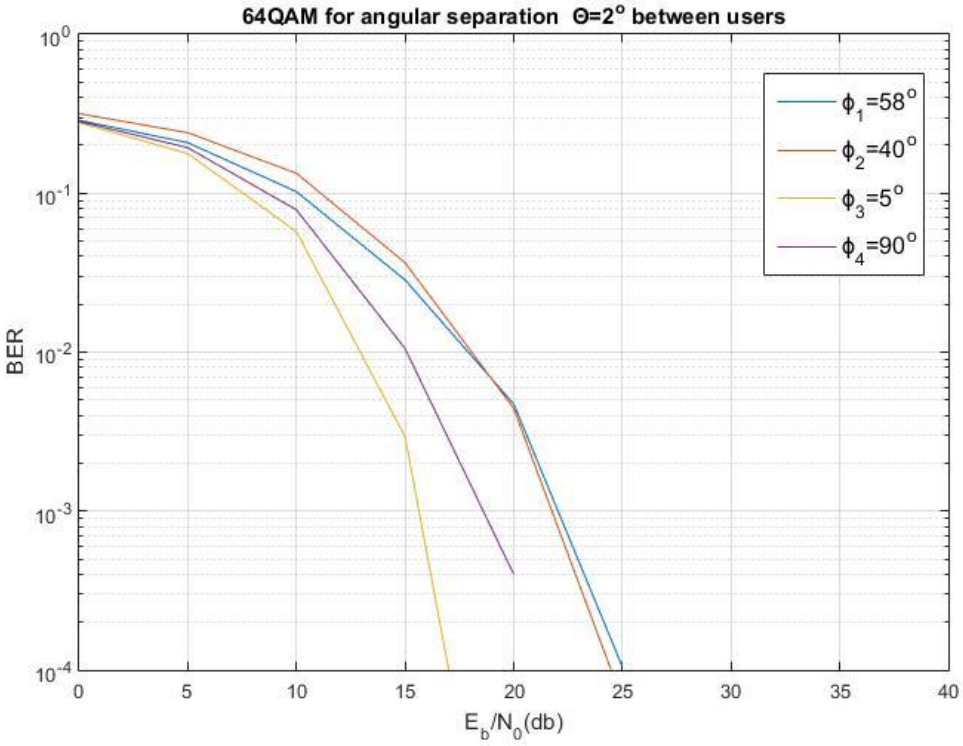

(a)

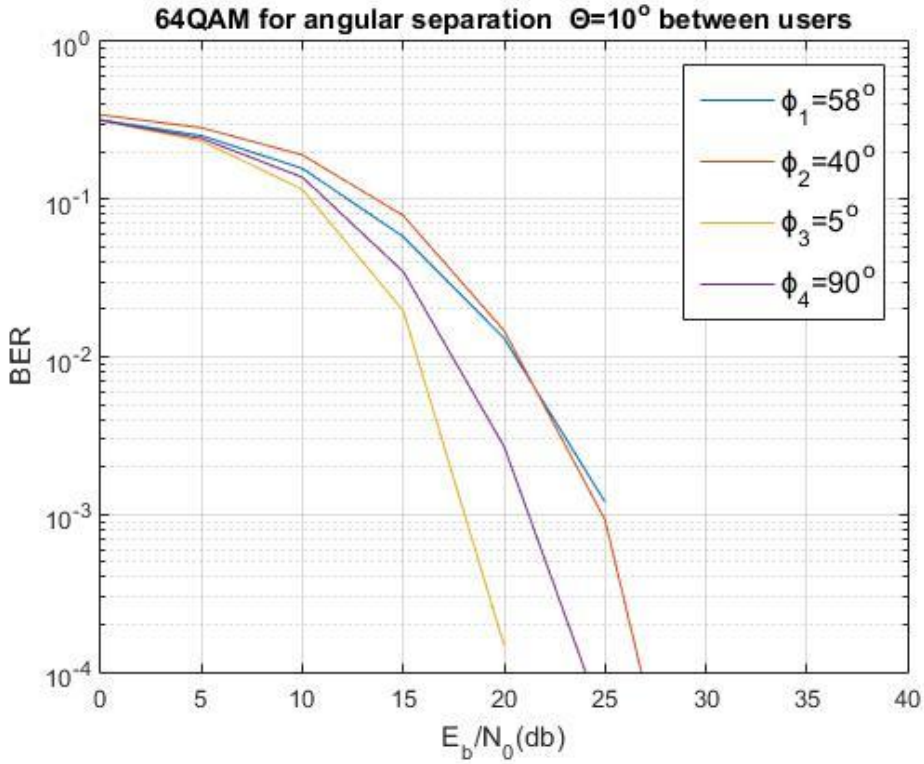

(b)

Figure 4.19 - System performance for 4 users for 64QAM for user separation $\Theta = 2^o$ (a) and $\Theta = 10^o$ (b)

As seen from the above figures, this transmitter structure is robust enough to support multiple users with physical layer security maintaining the same interference cancelation technique with decent performance.

5 Chapter V – Conclusions and future work

As future cellular systems continue to grow in demand of high quality of service, data rate and capacity, the development of new technologies is encouraged. In this thesis a new multilayer transmitter structure was proposed that, simultaneously, takes advantage of the millimeter wave spectrum and enables physical layer security.

5.1 Conclusions

Chapter II presented a brief context and introduction to 5G requirements and expectations, followed by an overview of the state of the art of the technologies that may form the core of the 5G networks, and that are also present in the proposed transmitter architecture.

Chapter III focus was on the characterization of antenna arrays and their effect on radiation directivity. The main objective here was to find the ideal size of the antenna array for the transmitter. Some interesting results were found for the 4 x 16 and 6 x 16 antenna arrays, which were taken as the basic antenna structures for the transmitter used in the following chapters.

Chapter IV begins by explaining an iterative DFE technique for SC-FDE schemes, proposed as a method to enhance amplification efficiency, deal with selective channels and mitigate ISI. This technique outperforms linear equalizers in dispersive channels and was used in all tested scenarios. This method is usually used at uplink scenarios, as the receiver is significantly more complex than the OFDM counterpart. Although not contemplated in this thesis, an ongoing project is studying the possibility of precoding the feedforward coefficient ($F_k^{(i)}$) at the transmitter for reduced receiver complexity. Also note that, as mentioned before, the main objective of this thesis is comparison between a regular beamforming transmitter with a double layer one, so the iterative aspect of the IB-DFE is not crucial in this context.

Secondly, the beamforming layer system model was explained and the impact of multiuser interference was studied. Imperfect beamforming was considered and user separation was not achieved, due to the occurrence of CCI. Since perfect CSI was assumed, a MMSE precoding interference cancellation technique was applied.

Section 4.5, described how any multilevel constellation can be decomposed into OQPSK or QPSK components, and then into $\log_2 M$ BPSK components, with M being the subsets of bits of the multilevel constellation. Section 4.6 applied this decomposition to the transmitter layer 1. Also, the evolution of MI was studied to see the effect of constellation's shaping for each optimization direction ϕ. It was found that for certain vicinities of ϕ, the MI has severe diminutions, indicating that small ϕ variations can result in severe loss of useful information. This property can be further analyzed to make the interception of data much harder for a possible eavesdropper.

Finally, the simulation results in section 4.6.3 considered a direct comparison between beamforming only and multi-layer transmitters for 16QAM and 64QAM constellations for a fully correlated channel. Results indicated that the double layer architecture, with the addition of efficient amplification and physical layer security reinforcement can be adopted without major penalties in performance. Then, the correlation effect between antennas of adjacent beamforming layers was studied and calculations exposed that an uncorrelated channel was not an unrealistic consideration. Results between both channel models (correlated and uncorrelated) presented a 6 dB improvement on BER performance in some cases. Lastly, an expansion of the system to support four users simultaneously was made and the transmitter structure revealed to be robust enough to support several users without any increased complexity.

5.2 Future work

The transmitter presented in this thesis can be used for further development and research. There are several ways to improve the system performance, for example, as mentioned before, the addition of multiple receiver antennas per user, which enables receive diversity. Another possible aspect is the addition of a nonlinear or successive precoding technique and the performance analysis of channel estimation.

An interesting study may be the use of other multilevel constellations and see the effect of ϕ estimation, perceiving the impact of ϕ estimation errors on overall performance. Additional testing must also be made to evaluate system performance for very large numbers of users.

References

[1] R. Wang, J. Cai, X. Yu, and S. Duan, “Disruptive Technologies and Potential Cellular Architecture for 5G,” *Open Electr. Electron. Eng. J.*, no. 9, pp. 512–517, 2015.

[2] F. Rusek, D. Persson, B. K. Lau, E. G. Larsson, T. L. Marzetta, O. Edfors, F. Tufvesson, Buon Kiong Lau, E. G. Larsson, T. L. Marzetta, and F. Tufvesson, “Scaling Up MIMO: Opportunities and Challenges with Very Large Arrays,” *IEEE Signal Process. Mag.*, vol. 30, no. 1, pp. 40–60, 2013.

[3] A. B. Gershman, N. D. Sidiropoulos, and S. Shahbazpanahi, “Convex Optimization-Based Beamforming,” *IEEE Signal Process. Mag.*, vol. 27, no. May, pp. 62–75, 2010.

[4] W. Li, T. Chang, C. Lin, and C. Chi, “Coordinated Beamforming for Multiuser MISO Interference Channel Under Rate Outage Constraints,” *IEEE Trans. Signal Process.*, vol. 61, no. 5, pp. 1087–1103, 2013.

[5] V. Astucia, P. Montezuma, R. Dinis, and M. Beko, “On the use of multiple grossly nonlinear amplifiers for highly efficient linear amplification of multilevel constellations,” *IEEE Veh. Technol. Conf.*, pp. 1–4, 2013.

[6] R. Dinis, P. Montezuma, P. Bento, M. Gomes, and V. Silva, “A Massive MIMO Architecture for Highly Efficient mm-wave Communications with Saturated Amplifiers,” in *Proc International Conf. on Electronics, Information and Communication - ICEIC, Singapore, Singapore*, 2015, pp. 1–5.

[7] Ericsson AB, “LTE - A 4G Solution,” *Ericsson White Pap.*, vol. 284 23-315, no. April, p. 9, 2011.

[8] X. Li, A. Gani, R. Salleh, and O. Zakaria, “The Future of Mobile Wireless Communication Networks,” *International Conference on Communication Software and Networks*. pp. 554–557, 2009.

[9] A. Osseiran, “Presentation - Mobile and wireless communications Enablers for the 2020 Information Society,” 2012, <https://www.metis2020.com/wpcontent/uploads/deliverables/METIS_project_presentation_public.pdf>.

[10] Ericsson, “5G Radio Access What is 5G ?,” *Ericsson White Pap.*, vol. 284. February, p. 10, 2015.

[11] J. G. J. G. Andrews, S. Buzzi, W. Choi, S. V. S. V. Hanly, A. Lozano, A. C. K. A. C. K. Soong, and J. C. J. C. Zhang, "What will 5G be?," *IEEE J. Sel. Areas Commun.*, vol. 32, no. 6, pp. 1065–1082, 2014.

[12] T. Cisco, "Cisco Visual Networking Index : Global Mobile Data Traffic Forecast Update , 2010 – 2015," *Cisco White Pap.*, vol. 2011, no. 4, pp. 2010–2015, 2011.

[13] A. Regalado, "How the Internet of Things Will Change Business | MIT Technology Review," *MIT Technol. Rev.*, 2014.

[14] M. Fallgren and B. Timus, "Scenarios, requirements and KPIs for 5G mobile and wireless system'','' *METIS Deliv. D*, vol. 1, p. 1, 2013.

[15] H. Benn, "Vision and Key Features for 5th Generation (5G) Cellular," *Samsung White Pap.*, January, pp. 1–25, 2014.

[16] R. I.-R. M.2078, "Estimated Spectrum Bandwidth Requirements for the Future Development of IMT-2000 and IMT-Advanced," 2006, < http://www.itu.int/dms_pub/itu-r/opb/rep/R-REP-M.2078-2006-PDF-E.pdf>.

[17] Agilent Technologies, "Wireless LAN at 60 GHz - IEEE 802 . 11ad Explained," 2013 < http://cp.literature.agilent.com/litweb/pdf/5990-9697EN.pdf>.

[18] Federal Communications Commission, "Millimeter Wave Propagation: Spectrum Management Implications," 1997, <http://scholar.google.com/scholar?hl=en&btnG=Search&q=intitle:Millimeter+Wave+Propagation+:+Spectrum+Management+Implications#0>.

[19] U. S. N. N. A. W. Center, *Electronic Warfare and Radar Systems Engineering Handbook*. Point Mugu, CA 93042, 1999, <http://www.navair.navy.mil/nawcwd/ewssa/downloads/NAWCWD%20TP%208347.pdf>.

[20] S. Rangan, T. S. Rappaport, and E. Erkip, "Millimeter-wave cellular wireless networks: Potentials and challenges," *Proc. IEEE*, vol. 102, no. 3, pp. 366–385, 2014.

[21] S. K. Mohapatra, B. R. Swain, N. Pati, and A. Pradhan, "Road Towards Mili Meter Wave Communication For 5G Network: A Technological Overview," *Trans. Mach. Learn. Artif. Intell.*, vol. 2, no. 3, pp. 48–60, 2014.

[22] T. S. Rappaport, Shu Sun, R. Mayzus, Hang Zhao, Y. Azar, K. Wang, G. N. Wong, J. K. Schulz, M. Samimi, and F. Gutierrez, "Millimeter Wave Mobile Communications for 5G Cellular: It Will Work!," *IEEE Access*, vol. 1, pp. 335–349, 2013.

[23] P. Kyösti, J. Meinilä, L. Hentilä, X. Zhao, T. Jämsä, C. Schneider, M. Narandzi, M. Milojevi, A. Hong, J. Ylitalo, V.-M. Holappa, M. Alatossava, R. Bultitude, Y. De Jong, and T. Rautiainen, "WINNER II Channel Models," 2008, < http://www.cept.org/files/1050/documents/winner2%20-%20final%20report.pdf>.

[24] H. P. Alliance, "HomePlug ™ AV2 Technology," *HomePlug AV2 White Pap.*, 2013.

[25] V. Tarokh, N. Seshadri, and a R. Calderbank, "Space-time codes for high data rate wireless communication: performance criterion and code construction," *Inf. Theory, IEEE Trans.*, vol. 44, no. 2, pp. 744–765, 1998.

[26] H. Lipfert, "MIMO OFDM Space Time Coding – Spatial Multiplexing Increasing Performance and Spectral Efficiency in Wireless Systems," 2007.

[27] S. Chen and J. Zhao, "The requirements, challenges, and technologies for 5G of terrestrial mobile telecommunication," *IEEE Commun. Mag.*, vol. 52, no. 5, pp. 36–43, 2014.

[28] D. Lee, H. Seo, B. Clerckx, E. Hardouin, D. Mazzarese, S. Nagata, and K. Sayana, "Coordinated multipoint transmission and reception in LTE-advanced: Deployment scenarios and operational challenges," *IEEE Commun. Mag.*, vol. 50, no. 2, pp. 148–155, 2012.

[29] B. Zid and R. Kosai, "Multi User MIMO Communication: Basic Aspects, Benefits and Challenges," in *Recent Trends in Multi-user MIMO Communications*, InTech, 2013, pp. 3–24.

[30] D. Gesbert, S. Hanly, H. Huang, S. Shamai Shitz, O. Simeone, and W. Yu, "Multi-Cell MIMO Cooperative Networks: A New Look at Interference," *IEEE J. Sel. Areas Commun.*, vol. 28, no. 9, pp. 1380–1408, Dec. 2010.

[31] T. L. Marzetta, "Noncooperative cellular wireless with unlimited numbers of base station antennas," *IEEE Trans. Wirel. Commun.*, vol. 9, no. 11, pp. 3590–3600, 2010.

[32] T. L. Marzetta, "How Much Training is Required for Multiuser Mimo?," in *2006 Fortieth Asilomar Conference on Signals, Systems and Computers*, 2006, pp. 359–363.

[33] W. Roh, J. Y. Seol, J. Park, B. Lee, J. Lee, Y. Kim, J. Cho, K. Cheun, and F. Aryanfar, "Millimeter-wave beamforming as an enabling technology for 5G cellular communications: Theoretical feasibility and prototype results," *IEEE Commun. Mag.*, vol. 52, no. 2, pp. 106–113, 2014.

[34] B. Razavi, “Design considerations for direct-conversion receivers,” *IEEE Trans. Circuits Syst. II Analog Digit. Signal Process.*, vol. 44, no. 6, pp. 428–435, 1997.

[35] S. Singh, R. Mudumbai, and U. Madhow, “Interference analysis for highly directional 60-GHz mesh networks: The case for rethinking medium access control,” *IEEE/ACM Trans. Netw.*, vol. 19, no. 5, pp. 1513–1527, 2011.

[36] B. Ng, C. T. Lam, and D. Falconer, “Turbo frequency domain equalization for single-carrier broadband wireless systems,” *IEEE Trans. Wirel. Commun.*, vol. 6, no. 2, pp. 759–767, 2007.

[37] B. K. Ng and D. Falconer, “A novel frequency domain equalization method for single-carrier wireless transmissions over doubly-selective fading channels,” in *IEEE Global Telecommunications Conference, 2004. GLOBECOM ’04.*, 2004, vol. 1, no. 1, pp. 237–241.

[38] H. S. Lui, H. T. Hui, and M. Bialkowski, “Mutual Coupling in Antenna Arrays,” *Int. J. Antennas Propag.*, vol. 2012, pp. 1–2, 2012.

[39] M. A. Zaman and M. Abdul Matin, “Nonuniformly Spaced Linear Antenna Array Design Using Firefly Algorithm,” *Int. J. Microw. Sci. Technol.*, vol. 2012, pp. 1–8, 2012.

[40] T. Yuan, N. Yuan, L.-W. Li, and M.-S. Leong, “Design and analysis of phased antenna array with low sidelobe by fast algorithm,” *Prog. Electromagn. Res.*, vol. 87, pp. 131–147, 2008.

[41] H. Oraizi and M. Fallahpour, “Nonuniformly spaced linear array design for the specified beamwidth/sidelobe level or specified directivity/sidelobe level with coupling considerations,” *Prog. Electromagn. Res. M*, vol. 4, pp. 185–209, 2008.

[42] M. A. Zaman and S. A. Mamun, “Phased Array Synthesis Using Modified Particle Swarm Optimization,” *J. Eng. Sci. Technol.*, vol. 4, no. 1, pp. 68–73, 2011.

[43] A. Ahmad, A. K. Behera, S. K. Mandal, G. K. Mahanti, and R. Ghatak, “Artificial bee colony algorithm to reduce the side lobe level of uniformly excited linear antenna arrays through optimized element spacing,” in *2013 IEEE Conference on Information and Communication Technologies*, 2013, pp. 1029–1032.

[44] M. Bisht and A. Joshi, “Various Techniques to Reduce PAPR in OFDM Systems: A Survey,” *Int. J. Signal Process. Image Process. Pattern Recognit.*, vol. 8, no. 11, pp. 195–206, Nov. 2015.

[45] H. Ochiai and H. Imai, “On clipping for peak power reduction of OFDM signals,” in *Globecom ’00 - IEEE. Global Telecommunications Conference. Conference Record (Cat. No.00CH37137)*, vol. 2, pp. 731–735.

[46] H. Joo, S. Heo, H. Jeon, J. No, and D.-J. Shin, “A New Blind SLM Scheme with Low Complexity of OFDM Signals,” in *2009 IEEE 70th Vehicular Technology Conference Fall*, 2009, no. 2, pp. 1–5.

[47] Dae-Woon Lim, Jong-Seon No, Chi-Woo Lim, and Habong Chung, “A new SLM OFDM scheme with low complexity for PAPR reduction,” *IEEE Signal Process. Lett.*, vol. 12, no. 2, pp. 93–96, Feb. 2005.

[48] J. S. Wang, J. H. Lee, J. C. Park, I. Song, and Y. H. Kim, “Combining of Cyclically Delayed Signals: A Low-Complexity Scheme for PAPR Reduction in OFDM Systems,” *IEEE Trans. Broadcast.*, vol. 56, no. 4, pp. 577–583, Dec. 2010.

[49] N. Benvenuto and S. Tomasin, “On the comparison between OFDM and single carrier modulation with a DFE using a frequency-domain feedforward filter,” *IEEE Trans. Commun.*, vol. 50, no. 6, pp. 947–955, Jun. 2002.

[50] N. Benvenuto and S. Tomasin, “Block iterative DFE for single carrier modulation,” *Electron. Lett.*, vol. 38, no. 19, p. 1144, 2002.

[51] M. Abdulrahman, A. U. H. Sheikh, and D. D. Falconer, “Decision feedback equalization for CDMA in indoor wireless communications,” *IEEE J. Sel. Areas Commun.*, vol. 12, no. 4, pp. 698–706, May 1994.

[52] Z. Tian, “Mitigating Error Propagation in Decision-Feedback Equalization for Multiuser CDMA,” *IEEE Trans. Commun.*, vol. 52, no. 4, pp. 525–529, Apr. 2004.

[53] H. Weingarten, Y. Steinberg, and S. Shamai, “The capacity region of the Gaussian multiple-input multiple-output broadcast channel,” *IEEE Trans. Inf. Theory*, vol. 52, no. 9, pp. 3936–3964, 2006.

[54] T. K. Y. Lo, “Maximum ratio transmission,” *IEEE Trans. Commun.*, vol. 47, no. 10, pp. 1458–1461, 1999.

[55] M. Joham, W. Utschick, and J. a. Nossek, “Linear transmit processing in MIMO communications systems,” *IEEE Trans. Signal Process.*, vol. 53, no. 8, pp. 2700–2712, 2005.

[56] E. Björnson, “Optimal Resource Allocation in Coordinated Multi-Cell Systems,” *Found. Trends® Commun. Inf. Theory*, vol. 9, no. 2–3, pp. 113–381, 2013.

[57] M. Costa, “Writing on dirty paper (Corresp.),” *IEEE Trans. Inf. Theory*, vol. 29, no. 3, pp. 439–441, May 1983.

[58] M. Tomlinson, “New automatic equaliser employing modulo arithmetic,” *Electron. Lett.*, vol. 7, no. 5–6, p. 138, 1971.

[59] H. Harashima and H. Miyakawa, “Matched-transmission technique for channels with intersymbol interference,” *IEEE Trans. Commun.*, vol. 20, no. 4, pp. 774–780, 1972.

[60] B. M. Hochwald, C. B. Peel, and A. L. Swindlehurst, “A vector-perturbation technique for near-capacity multiantenna multiuser communication - Part II: Perturbation,” *IEEE Trans. Commun.*, vol. 53, no. 3, pp. 537–544, 2005.

[61] P. Montezuma, “Design of TC-OQAM schemes using a generalised nonlinear OQPSK-type format,” *Electron. Lett.*, vol. 35, no. 11, p. 860, 1999.

[62] P. Montezuma and R. Dinis, “Implementing Physical Layer Security Using Transmitters with Constellation Shaping,” in *2015 24th International Conference on Computer Communication and Networks (ICCCN)*, 2015, pp. 1–4.

[63] C. E. Shannon, “A Mathematical Theory of Communication,” *Bell Syst. Tech. J.*, vol. 27, no. 3, pp. 379–423, 1948.

[64] A. Guillén i Fàbregas, A. Martinez, and G. Caire, “Bit-Interleaved Coded Modulation,” *Found. Trends® Commun. Inf. Theory*, vol. 5, no. 1–2, pp. 1–153, 2007.

[65] E. A. Jorswieck and H. Boche, “Optimal Transmission Strategies and Impact of Correlation in Multiantenna Systems with Different Types of Channel State Information,” *IEEE Trans. Signal Process.*, vol. 52, no. 12, pp. 3440–3453, Dec. 2004.

[66] A. M. Tulino, A. Lozano, and S. Verdu, “Impact of Antenna Correlation on the Capacity of Multiantenna Channels,” *IEEE Trans. Inf. Theory*, vol. 51, no. 7, pp. 2491–2509, Jul. 2005.

[67] Da-Shan Shiu, G. J. Foschini, M. J. Gans, and J. M. Kahn, “Fading correlation and its effect on the capacity of multielement antenna systems,” *IEEE Trans. Commun.*, vol. 48, no. 3, pp. 502–513, Mar. 2000.

[68] S. Blanch, J. Romeu, and I. Corbella, “Exact representation of antenna system diversity performance from input parameter description,” *Electron. Lett.*, vol. 39, no. 9, p. 705, 2003.